

YITP-SB-02-32

INLO-PUB-4/02

NLO differential distributions of massive lepton-pair production in longitudinally polarized proton-proton collisions

V. RAVINDRAN

*Harish-Chandra Research Institute,
Chhatnag Road, Jhansi,
Allahabad, 211019, India.*

J. SMITH ¹

*C.N. Yang Institute for Theoretical Physics,
State University of New York at Stony Brook, New York 11794-3840, USA.*

W.L. VAN NEERVEN ²

*Instituut-Lorentz
University of Leiden,
PO Box 9506, 2300 RA Leiden,
The Netherlands.*

June 2002

Abstract

We present the full next-to-leading order (NLO) corrected inclusive cross section $d^3\Delta\sigma/dQ^2/dy/dp_T$ for massive lepton pair production in longitudinally polarized proton-proton collisions $p+p \rightarrow l^+l^- + 'X'$. Here $'X'$ denotes any inclusive hadronic state and Q represents the invariant mass of the lepton pair which has transverse momentum p_T and rapidity y . All QCD partonic subprocesses have been included provided the lepton pair is created by a virtual photon, which is a valid approximation for $Q < 50$ GeV. Like in unpolarized proton-proton scattering the dominant subprocess is given by $q(\bar{q}) + g \rightarrow \gamma^* + 'X'$ so that massive lepton pair production provides us with an excellent method to measure the spin density of the gluon. Our calcu-

¹partially supported by the National Science Foundation grant PHY-0098527.

²Work supported by the EC network 'QCD and Particle Structure' under contract No. FMRX-CT98-0194.

lations are carried out using the method of n -dimensional regularization by making a special choice for the γ_5 -matrix. Like in the case of many other prescriptions evanescent counter terms appear. They are determined by computing the NLO coefficient functions for $d\Delta\sigma/dQ^2$ and the polarized cross section for Higgs production using both n -dimensional regularization and a four dimensional regularization technique in which the γ_5 -matrix is uniquely defined. Our calculations reveal that the non-singlet polarized coefficient function equals the unpolarized one up to a minus sign. We give predictions for double longitudinal spin asymmetry measurements at the RHIC.

PACS numbers: 12.38.Bx, 12.38.Qk, 13.85.Qk

1 Introduction

With the advent of the RHIC at BNL we have a new facility to study the spin structure of the proton, (for a review on the potential of RHIC see [1]), which supplements the existing polarized lepton-hadron machines. Polarized proton-proton collisions with a very high luminosity and a maximum centre of mass energy of $\sqrt{s} = 500$ GeV will provide us with many more details about spin distributions than possible with the existing lepton-hadron machines, which give very little information about the polarized gluon and sea-quark parton densities. An exception is photo-production of heavy flavours where the virtual photon is almost on-shell. This process allows us to measure the polarized gluon density and has been calculated up to next-to-leading order (NLO) in [2]. The gluon density can also be extracted from data on prompt photon production, heavy flavour production and massive lepton pair production (Drell-Yan or DY process) in proton-proton collisions. The DY reaction also provides information on the polarized sea-quark densities. In order to measure these densities the above reactions have to be calculated at least up to NLO in perturbative QCD. This has been achieved for prompt photon production in [3], [4] and for heavy flavour production in [5]. Up to the same order calculations have been done for the polarized cross section $d^2\Delta\sigma/dQ^2/dy$ of the Drell-Yan (DY) process in [6] and [7]. Vector boson production in NLO for the cross section $d\Delta\sigma/dQ^2$ has been studied in [8]. Notice that these DY cross sections provide us with information about the sea-quark density rather than about the gluon density. To determine the latter one needs to study the differential distribution $d^3\Delta\sigma/dQ^2/dy/dp_T$ where the transverse momentum p_T is sufficiently large so that the quark-gluon (qg) subprocess dominates the quark-anti-quark ($q\bar{q}$) subprocess. According to studies in [9] and [10] this already occurs for $p_T > Q/2$. Notice that the quark-gluon subprocess also dominates in prompt photon production at large p_T . This reaction has a much larger cross section than the one for the DY process, which behaves like $1/Q^4$ at large Q so one might favour it. However the former reaction also has its disadvantages, as we have already seen for unpolarized prompt photon production, due to experimental and theoretical complications with photon isolation criteria. Moreover the DY process has an additional large scale represented by the lepton pair mass Q which turns out to be a much better scale to use than p_T . The NLO QCD corrections for the unpolarized DY cross section $d^3\sigma/dQ^2/dy/dp_T$ were performed in [11]

(non-singlet) and in [12] (singlet). A complete NLO QCD calculation for the polarized cross section does not exist yet except for the non-singlet part computed in [13], [14]. One can show, using general arguments, that apart from a minus sign the non-singlet DY coefficient function due to the $q\bar{q}$ -channel should be equal to its unpolarized analogue.

In this paper we present a complete NLO calculation of the polarized DY cross section $d^3\Delta\sigma/dQ^2/dy/dp_T$ where all partonic subprocesses are included. Our findings for the non-singlet coefficient function agree with those obtained in [13], [14] and they confirm the relation stated above. In the past most of the corrections to physical quantities were performed using the method of n -dimensional regularization [16] to define the singularities which occur in loop and phase space integrals. This method was preferred above other regularization techniques because it manifestly preserves the Ward-identities in non-abelian gauge field theories like QCD. However this advantage gets lost when one has to deal with the γ_5 -matrix and the Levi-Civita tensor which appear in the electroweak standard model and in QCD when one studies polarization effects. In this case some Ward identities are violated and have to be restored by the addition of so-called evanescent counter terms. There exists a large literature about the γ_5 -matrix and the Levi-Civita tensor in the context of ultraviolet divergences (see [15]) but a thorough study on how to handle collinear and infrared singularities, which are characteristic of partonic cross sections, is still lacking. The most often used prescription to compute polarized partonic cross sections is called HVBM after the initials of the authors in [16] and [17]. As is shown in [18]- [22] this prescription also requires that evanescent counter terms have to be taken into account otherwise one gets wrong coefficient functions. In practice it turns out that the computation of higher order corrections to physical quantities in the HVBM prescription is more complicated than the usual n -dimensional regularization technique. This can be attributed to the split up of the n -dimensional space in a 4 and an $n - 4$ dimensional subspace. Accordingly the gamma-matrices and the momenta have to split up which complicates the gamma-matrix algebra and the phase space integrals. To avoid this we introduce in this paper a prescription for the γ_5 -matrix which is easier to implement in computer algebra programs which do not contain a package to deal with gamma-matrices following the HVBM prescription. Moreover the n -dimensional phase space integrals take their usual form as in calculations where the γ_5 -matrix is not present. The evanescent counter terms which we need in our NLO calcula-

tion of $d^3\Delta\sigma/dQ^2/dy/dp_T$ are extracted from an NLO computation of the DY polarized differential cross section $d\Delta\sigma/dQ^2$ and from the Higgs boson polarized total cross section. To check our procedure we re-calculate these coefficient functions using a four dimensional regularization technique (see e.g. [23]) where the γ_5 -matrix is uniquely defined.

Our paper is organized as follows. In section 2 we introduce our notations and discuss extensively the technicalities which are involved if one wants to give a prescription for the γ_5 -matrix using n -dimensional regularization. We introduce our own definition and determine the corresponding evanescent counter terms by comparing our results with those obtained by four dimensional regularization techniques. In section 3 we present the NLO corrections to the differential polarized DY cross section and check the coefficient functions by re-calculating them in a four dimensional regularization method. In section 4 we study the NLO corrections to polarized DY production in proton-proton collisions at RHIC and make a comparison with earlier results which were obtained in LO only. The long formulae for the soft-plus-virtual gluon contributions to the coefficient functions can be found in Appendix A.

2 Lowest order contributions to the polarized Drell-Yan process

In this paper we consider the semi-inclusive Drell-Yan process

$$\begin{aligned}
 H_1(P_1, S_1) + H_2(P_2, S_2) &\rightarrow \gamma^*(q) + 'X', \\
 &\quad \quad \quad | \\
 &\quad \quad \quad \rightarrow l^+(l_1) + l^-(l_2)
 \end{aligned}$$

$$S = (P_1 + P_2)^2, \quad Q^2 \equiv q^2 = (l_1 + l_2)^2, \quad (2.1)$$

where H_i ($i = 1, 2$) represent the incoming polarized hadrons carrying the momenta P_i and spins S_i . Further $'X'$ denotes any inclusive hadronic state which is unpolarized. The lepton pair is represented by l^+l^- with momenta l_1, l_2 . In this paper we will only consider lepton pairs which have a sufficiently small invariant mass Q so that the photon dominates in the above reaction and Z -boson exchange effects can be neglected. In addition to the kinematical variables in Eq. (2.1) we need the following variables

$$T = (P_1 - q)^2, \quad U = (P_2 - q)^2, \quad (2.2)$$

to obtain the differential cross section

$$S^2 \frac{d^3 \Delta\sigma^{\text{H}_1\text{H}_2}}{dQ^2 dT dU}(S, T, U, Q^2) = \frac{4\pi\alpha^2}{3Q^2} S \frac{d^2 \Delta W^{\text{H}_1\text{H}_2}}{dT dU}(S, T, U, Q^2). \quad (2.3)$$

In the QCD improved parton model the hadronic DY structure function $d\Delta W^{\text{H}_1\text{H}_2}$ is related to the partonic structure function $d\Delta W_{ab}$ as follows

$$\begin{aligned}
 &S \frac{d^2 \Delta W^{\text{H}_1\text{H}_2}}{dT dU}(S, T, U, Q^2) \\
 &= \sum_{a_1, a_2=q, \bar{q}, g} \int_{x_{1,\min}}^1 \frac{dx_1}{x_1} \int_{x_{2,\min}}^1 \frac{dx_2}{x_2} \Delta f_{a_1}^{\text{H}_1}(x_1, \mu^2) \Delta f_{a_2}^{\text{H}_2}(x_2, \mu^2) \\
 &\quad \times s \frac{d^2 \Delta W_{a_1 a_2}}{dt du}(s, t, u, Q^2, \mu^2). \quad (2.4)
 \end{aligned}$$

In the formula above $\Delta f_a(x, \mu^2)$ ($a = q, \bar{q}, g$) are the polarized parton probability densities where μ denotes the factorization/renormalization scale and

x is the fraction of the hadron momentum carried away by the parton. The DY partonic structure function $d^2\Delta W_{a_1 a_2}$ is computed from the partonic subprocess

$$a_1(p_1, s_1) + a_2(p_2, s_2) \rightarrow \gamma^*(q) + b_1(k_1) \cdots b_m(k_m) \quad (2.5)$$

and it reads

$$\begin{aligned} \Delta W_{a_1 a_2} &= K_{a_1 a_2} \int d^4q \delta(q^2 - Q^2) \\ &\times \prod_{i=1}^m \int \frac{d^3k_i}{(2\pi)^3 2E_i} \delta^{(4)}\left(p_1 + p_2 - q - \sum_{j=1}^m k_j\right) \\ &\times |\Delta M_{a_1 + a_2 \rightarrow \gamma^* + b_1 \cdots b_m}|^2, \end{aligned} \quad (2.6)$$

where $K_{a_1 a_2}$ denotes the colour and spin average factor and the polarized matrix elements are denoted ΔM (when we refer to unpolarized structure functions, matrix elements and parton densities we drop the Δ). The partonic kinematical variables are defined in analogy with the hadronic variables in Eqs. (2.1), (2.2) as

$$s = (p_1 + p_2)^2, \quad t = (p_1 - q)^2, \quad u = (p_2 - q)^2. \quad (2.7)$$

In the case parton p_1 emerges from hadron $H_1(P_1)$ and parton p_2 emerges from hadron $H_2(P_2)$ we can establish the following relations

$$\begin{aligned} p_1 &= x_1 P_1, & p_2 &= x_2 P_2, \\ s &= x_1 x_2 S, & t &= x_1(T - Q^2) + Q^2, & u &= x_2(U - Q^2) + Q^2, \\ x_{1,\min} &= \frac{-U}{S + T - Q^2}, & x_{2,\min} &= \frac{-x_1(T - Q^2) - Q^2}{x_1 S + U - Q^2}. \end{aligned} \quad (2.8)$$

When parton p_1 emerges from hadron $H_2(P_2)$ and parton p_2 emerges from $H_1(P_1)$ one obtains the same expression as in Eq. (2.4) except that T and U are interchanged. This result has to be added to Eq. (2.4). When the partonic cross section is symmetric under $t \leftrightarrow u$ one can also use the representation in Eq. (2.4) without adding the result where T and U are interchanged

provided one makes the replacement $\Delta f_{a_1}^{\text{H}_1} \Delta f_{a_2}^{\text{H}_2} \rightarrow \Delta f_{a_1}^{\text{H}_1} \Delta f_{a_2}^{\text{H}_2} + \Delta f_{a_1}^{\text{H}_2} \Delta f_{a_2}^{\text{H}_1}$. Finally note that the relation between the parton probability densities above and the parton momentum densities appearing in the parton density sets in the literature or PDF libraries, which are denoted by $\Delta f_a^{\text{PDF}}(x, \mu^2)$, is given by $\Delta f_a^{\text{PDF}}(x, \mu^2) = x \Delta f_a(x, \mu^2)$.

When $|\Delta M_{a_1 a_2}|^2$ in Eq. (2.6) is calculated up to order α_s^2 one encounters four partonic subprocesses which are characterised by the two partons in their initial state. In the case of quarks with a mass $m \neq 0$ they are given by

$$q(p_1, s_1) + \bar{q}(p_2, s_2) \rightarrow \gamma^* + X',$$

$$|\Delta M_{q\bar{q}}|^2 = \frac{1}{4} \mathbf{Tr} \left(\gamma_5 \not{\epsilon}_2 (\not{p}_2 - m) \tilde{M} \gamma_5 \not{\epsilon}_1 (\not{p}_1 + m) \tilde{M}^\dagger \right), \quad (2.9)$$

$$q_1(\bar{q}_1)(p_1, s_1) + g(p_2) \rightarrow \gamma^* + X',$$

$$|\Delta M_{qg}|^2 = \frac{1}{4} \epsilon_{\mu\nu\lambda\sigma} \frac{p_2^\lambda l_2^\sigma}{p_2 \cdot l_2} \mathbf{Tr} \left(\tilde{M}^\mu \gamma_5 \not{\epsilon}_1 (\not{p}_1 \pm m) \tilde{M}^{\nu\dagger} \right), \quad (2.10)$$

$$q_1(\bar{q}_1)(p_1, s_1) + q_2(\bar{q}_2)(p_2, s_2) \rightarrow \gamma^* + X'$$

$$|\Delta M_{q_1 q_2}|^2 = \frac{1}{4} \mathbf{Tr} \left(\gamma_5 \not{\epsilon}_2 (\not{p}_2 \pm m) \tilde{M} \gamma_5 \not{\epsilon}_1 (\not{p}_1 \pm m) \tilde{M}^\dagger \right), \quad (2.11)$$

$$g(p_1) + g(p_2) \rightarrow \gamma^* + X',$$

$$|\Delta M_{gg}|^2 =$$

$$\frac{1}{4} \epsilon_{\mu_2 \nu_2 \lambda_2 \sigma_2} \frac{p_2^{\lambda_2} l_2^{\sigma_2}}{p_2 \cdot l_2} \epsilon_{\mu_1 \nu_1 \lambda_1 \sigma_1} \frac{p_1^{\lambda_1} l_1^{\sigma_1}}{p_1 \cdot l_1} \mathbf{Tr} \left(\tilde{M}^{\mu_1 \mu_2} \tilde{M}^{\nu_1 \nu_2 \dagger} \right), \quad (2.12)$$

where \tilde{M} denotes the matrix element which is given by the standard Feynman rules. Further the symbol \mathbf{Tr} can represent multiple traces when the matrix elements are calculated in higher order and for the reaction in Eq. (2.11) one can distinguish between $q_1 = q_2$ and $q_1 \neq q_2$. The spin vectors s_i and the gauge vectors l_i ($i = 1, 2$) satisfy the properties

$$s_i \cdot p_i = 0, \quad s_i \cdot s_i = -1, \quad l_i \cdot l_i = 0. \quad (2.13)$$

When the (anti-)quark is massless then one has to make the replacements

$$\gamma_5 \not{\epsilon}_i (\not{p}_i \pm m) \rightarrow \pm \gamma_5 h_i \not{p}_i, \quad (2.14)$$

where h_i ($i = 1, 2$) represent the helicities of the incoming (anti-)quarks and the $+$ and $-$ signs on the righthand side hold for the quarks and anti-quarks respectively. The definitions above are chosen in such a way that the partonic polarized structure function satisfies the property

$$\Delta W_{a_1 a_2} = W_{a_1 a_2}(+, +) - W_{a_1 a_2}(+, -), \quad (2.15)$$

with $+, -$ denoting the helicities of the incoming partons.

The computation of the matrix elements in Eqs. (2.9)-(2.12) and their virtual corrections reveals divergences which occur when the momenta over which one integrates tend to zero (infrared), infinity (ultraviolet) or collinear to another momentum (collinear). The most popular way to regularize these singularities is to choose the method of n -dimensional regularization [16] in which the space is extended to n dimensions. The singularities are represented by pole terms of the type $(1/\varepsilon)^k$ with $n = 4 + \varepsilon$. This method is very useful because it preserves the Ward identities in the case of gauge theories. However this is no longer the case when the γ_5 matrix and the Levi-Civita tensor appear like in Eqs. (2.9)-(2.12) or in weak interactions. There is no consistent way to generalize these two quantities in n dimensions contrary to the ordinary matrix γ_μ or the metric tensor $g_{\mu\nu}$. In the literature one has proposed various methods to extend the γ_5 matrix and the Levi-Civita tensor to n dimensions but one always needs so-called evanescent counter terms to restore the Ward identities. A very popular prescription is the HVBM-scheme which was proposed in [16] and generalised in [17]. In this approach the gamma-matrices and the momenta have to be split up into a 4 and an $n - 4$ dimensional part. Therefore also the integrals over the final state momenta have to split up in the same way. Many NLO calculations have been done in this scheme (see e.g. [2]-[8], [13], [14]). However this approach requires a special procedure to deal with the gamma-matrix algebra which is not implemented in the program FORM [24]. Since this program is used in our calculations we prefer another prescription for the γ_5 -matrix which is given in [25]. It gives the same results as the HVBM-scheme but it is much simpler to use in algebraic manipulation programs. Moreover one does not have to split up the integrals over the final state momenta and one

can simply use the phase space integrals computed for unpolarized reactions (see e.g. [26]). The procedure in [25] is given by

1. Replace the γ_5 -matrix by

$$\gamma_\mu \gamma_5 = \frac{i}{6} \epsilon_{\mu\rho\sigma\tau} \gamma^\rho \gamma^\sigma \gamma^\tau \quad \text{or} \quad \gamma_5 = \frac{i}{24} \epsilon_{\rho\sigma\tau\kappa} \gamma^\rho \gamma^\sigma \gamma^\tau \gamma^\kappa.$$

2. Compute all matrix elements in n dimensions.
3. Evaluate all Feynman integrals and phase space integrals in n -dimensions.
4. Contract the Levi-Civita tensors in four dimensions after the Feynman integrals and phase space integrals are carried out.

(2.16)

Note that the contraction in four dimensions only applies to Lorentz indices which are present in the Levi-Civita tensors. The last step in (2.16) requires that one first has to apply tensorial reduction to all integrals. For simple expressions this takes the form

$$\begin{aligned} \int \frac{d^n k}{(2\pi)^n} k^\mu k^\nu f(k, p_1, p_2) &= A_{00}(n) g^{\mu\nu} + A_{11}(n) p_1^\mu p_1^\nu + A_{22}(n) p_2^\mu p_2^\nu \\ &\quad + A_{12}(n) p_1^\mu p_2^\nu + A_{21}(n) p_2^\mu p_1^\nu, \end{aligned}$$

$$\begin{aligned} \int dPS^{(2)} k^\mu k^\nu f(k, p_1, p_2) &= B_{00}(n) g^{\mu\nu} + B_{11}(n) p_1^\mu p_1^\nu + B_{22}(n) p_2^\mu p_2^\nu \\ &\quad + B_{12}(n) p_1^\mu p_2^\nu + B_{21}(n) p_2^\mu p_1^\nu, \end{aligned}$$

(2.17)

where the coefficients A_{ij}, B_{ij} depend on $n = 4 + \varepsilon$. The HVBM-scheme or the prescription above automatically reproduces the Adler-Bell-Jackiw anomaly (ABJ) [27] but it violates the Ward identity for the non-singlet axial vector current and the Adler-Bardeen theorem [28]. In order to obtain the correct renormalized quantities one therefore needs to invoke additional counter terms [18], which are called evanescent since they do not occur for

$n = 4$. This procedure was used to obtain the NLO anomalous dimensions for the spin operators which determine the evolution of the parton spin densities see [19], [20]. Notice that in our case the Drell-Yan process only involves one photon exchange. Therefore the γ_5 -matrix does not appear in the virtual amplitude so that there is no problem in the ultraviolet sector. Evanescent counter terms are also needed in cases where collinear divergences show up like in partonic cross sections (see e.g. [22]). This is characteristic for the HVBM scheme as well as any other approach similar to the one we propose later on. The reason is that in n -dimensional regularization there exists a one-to-one correspondence between the ultraviolet divergences occurring in partonic operator matrix elements and the collinear divergences appearing in partonic cross sections provided both quantities are of twist two type. The main problem with each prescription to extend the γ_5 -matrix and the Levi-Civita tensor beyond 4 dimensions is that one does not know beforehand which Ward identities are violated. Hence in principle all $\varepsilon = n - 4$ terms in the matrix element might be spurious so that one is never sure to obtain the correct result. An example is the spurious terms occurring in the interference terms in the quark-quark channel which are discussed below Eq. (3.15).

A way to avoid this problem is to drop n -dimensional regularization and to resort to four dimensional regularization techniques where the γ_5 -matrix anti-commutes with the other γ_μ matrices and the Levi-Civita tensor is clearly defined. However four dimensional regularization methods have their drawbacks too because they also violate Ward identities in particular in the ultraviolet sector where it is difficult to apply techniques like Pauli-Villars [29] or the introduction of an ultraviolet cut off on the divergent integrals. In the case of collinear and infrared divergences four dimensional techniques have been applied in a more successful way provided certain rules are respected. In [23] it was shown that off-shell and on-shell regularization leads to the same coefficient functions as those found by using n -dimensional regularization as regards the NLO unpolarized DY total cross section. In [30] the same result was shown for the process $q + q \rightarrow q + q + \gamma^*$ where the NNLO coefficient function agrees with the one obtained by the off-shell and on-shell techniques applied in [31]. The off-shell and on-shell regularization techniques are defined by (see Eqs. (2.9)-(2.12))

off-shell

$$p_i \cdot p_i = p_i^2 < 0, \quad m = 0,$$

p_i represents the quark as well as the gluon momentum ,

on-shell

$$p_i \cdot p_i = m^2 \neq 0, \quad p_i \text{ is the quark momentum ,}$$

$$p_i \cdot p_i = 0, \quad p_i \text{ is the gluon momentum .} \tag{2.18}$$

The on-shell technique has the advantage that the partonic cross sections are gauge invariant like the ones computed by n -dimensional regularization, where the mass m is set to be zero. The disadvantage is that the collinear and infrared divergences due to the gluon have to be regularized by a different technique. The off-shell regularization is universal both for gluons and quarks but the partonic cross sections depend on the chosen gauge. However the same gauge dependence also appears in the operator matrix elements so that it cancels in the coefficient functions after subtraction of the former from the partonic cross sections. This is checked for the cases mentioned above Eq. (2.18). A more serious drawback is that one has to be very cautious when collinear and infrared divergences appear together which happens in the virtual and soft gluon corrections. As was shown in [23] the off-shell assignment as given in Eq. (2.18) leads to the wrong coefficient function unless it is computed in the axial gauge (see [32]). Therefore in the case of the virtual and soft gluon corrections one has to introduce a more sophisticated off-shell regularization which respects the Kinoshita double cutting rules as formulated in [33]. In the case when only collinear divergences appear, which happens in radiative processes, the off-shell regularization in Eq. (2.18) can be successfully applied.

We will use in parallel two regularization techniques to compute the NLO corrections to the double differential structure function in Eq. (2.3). This allows us to overcome the above problems associated with all the regularization techniques and with the evanescent counter terms which have to be introduced in the case of n -dimensional regularization. For the first method

we adopt a prescription which is slightly different from HVBM in Eq. (2.16), namely

1. Replace the γ_5 -matrix in by

$$\gamma_\mu \gamma_5 = \frac{i}{6} \epsilon_{\mu\rho\sigma\tau} \gamma^\rho \gamma^\sigma \gamma^\tau \quad \text{or} \quad \gamma_5 = \frac{i}{24} \epsilon_{\rho\sigma\tau\kappa} \gamma^\rho \gamma^\sigma \gamma^\tau \gamma^\kappa.$$

2. Compute all matrix elements in n dimensions.
3. Evaluate all Feynman integrals and phase space integrals in n dimensions.
4. Contract the Levi-Civita tensors in four dimensions after the Feynman integrals and soft gluon phase space integrals are done.
5. Contract the Levi-Civita tensors in four dimensions first before the hard gluon phase space integrals are carried out

(2.19)

Note that by hard gluon phase space integrals we mean all integrals where we do not encounter infrared divergences. In the subsequent part of this paper we will call this version of n -dimensional regularization the RSN-scheme. It only differs from the scheme in Eq. (2.16) regarding the procedure in contracting the Levi-Civita tensors. We have chosen this approach to avoid tensorial reduction of the hard gluon phase space integrals in n dimensions as is needed for the scheme in Eq. (2.16) which is equivalent to the HVBM-scheme. For the virtual corrections we can simply use the method of tensorial reduction of the Feynman integrals into scalar integrals which is presented in [34] and [35]. Notice that the soft gluon contributions have to be treated in the same way as the virtual corrections because they have to be added in order to cancel the final state collinear and infrared divergences in the final result. Because there are only a few soft gluon phase space integrals, their tensorial reduction is feasible. A drawback of the RSN approach is that one has to compute many more evanescent counter terms than in the case of the HVBM-scheme. These terms will be extracted from the computation of the completely integrated NLO structure function which is one order lower in α_s

than the NLO correction to the double differential structure function in Eq. (2.3). The reason that n -dimensional integration and the contraction of the Levi-Civita tensors in four dimensions do not commute can be attributed to the metric tensor $g_{\mu\nu}$ in Eq. (2.17). When the integration is performed first $g_{\mu\nu}$ acts as an n -dimensional object which is indicated by the dependence of the coefficients of $A_{ij}(n)$ and $B_{ij}(n)$ in Eq. (2.17) on n . When the contraction is done first in four dimensions all metric tensors appearing in the matrix elements are four dimensional objects provided they have the same Lorentz indices in common with the Levi-Civita tensors. This explains the difference between the HVBM and the RSN scheme. We checked that in the latter scheme $|\Delta M_{qg}|^2$ in Eq. (2.10) does not depend on the gauge vector l_2 . This independence persists if one adds an unpolarized gluon in the final state with gauge vector l to the lower order processes in Eqs. (2.9), (2.10) where the sum over the physical polarizations is given by

$$P^{\mu\nu}(l, p) \equiv \sum_{\alpha=L,R} \epsilon^\mu(p, \alpha) \epsilon^\nu(p, \alpha) = -g^{\mu\nu} + \frac{l^\mu p^\nu + l^\nu p^\mu}{l \cdot p}. \quad (2.20)$$

The polarization sum above satisfies the conditions

$$l_\mu P^{\mu\nu} = P^{\mu\nu} l_\nu = 0, \quad l^2 = 0. \quad (2.21)$$

There is one exception. If there are two polarized gluons in the initial state like in reaction (2.12) it turns out that $|\Delta M_{gg}|^2$ depends on l_1 and l_2 so that one has to make a specific choice for them. In this paper we will choose $l_1 = p_2$ and $l_2 = p_1$. In order to check the RSN method for the computation of the $2 \rightarrow 3$ body hard gluon processes we compute the double differential partonic structure function in four dimensions using the off-shell regularization technique in Eq. (2.18). This will be our second regularization method.

In the final part of this section we have to compute the evanescent counter terms which show up in the RSN-scheme. They are extracted from the NLO totally integrated structure function in Eq. (2.6) which has to be computed using several regularization schemes. Here we assume that only four dimensional regularization techniques provide us with the proper answer since the γ_5 -matrix anti-commutes with the other γ_μ -matrices. On the Born level we have the following partonic subprocesses (see Eq. (2.5))

$$q(p_1) + \bar{q}(p_2) \rightarrow \gamma^*, \quad g(p_1) + g(p_2) \rightarrow H, \quad (2.22)$$

where H represents a scalar particle e.g. the Higgs boson which like the photon has a mass indicated by the same variable Q . The reason that we need the latter process is that the totally integrated DY structure function in NLO only provides us with information about the splitting functions ΔP_{qq} and ΔP_{qg} but we also need to know ΔP_{gq} and ΔP_{gg} which can be extracted from scalar boson production. In lowest order the matrix elements are

$$|\Delta M_{q\bar{q}\rightarrow\gamma^*}^{(0)}|^2 = -N s \left(1 - \frac{\varepsilon}{2}\right), \quad |\Delta M_{gg\rightarrow H}^{(0)}|^2 = -\frac{1}{8} (N^2 - 1) s^2, \quad (2.23)$$

where N denotes the number of colours. The reason that the latter matrix element has one power in s more than the former can be attributed to the effective scalar-gluon-gluon coupling which has a dimension which is equal to the inverse of a mass. This coupling like the electromagnetic coupling in $|\Delta M_{q\bar{q}\rightarrow\gamma^*}^{(0)}|^2$ has not been included in the definition of ΔW . On the Born level the polarized structure functions become

$$\Delta W_{q\bar{q}}^{(0)} = -\frac{1}{N} \delta(1-x), \quad \Delta W_{gg}^{(0)} = -\frac{1}{N^2-1} \delta(1-x), \quad x = \frac{Q^2}{s}. \quad (2.24)$$

Notice that for the DY process we have divided by $1 - \varepsilon/2$ whereas for scalar particle production we have removed an overall term $Q^2/8$ in order to get unity on the right hand side of $\Delta W_{q\bar{q}}^{(0)}$ and $\Delta W_{gg}^{(0)}$ respectively. In NLO the matrix elements in the RSN scheme as well as in the off-shell mass scheme read

$$\begin{aligned} q(p_1) + \bar{q}(p_2) &\rightarrow g(k_1) + \gamma^*(q), \\ |\Delta M_{q\bar{q}\rightarrow g \gamma^*}^{(1)}|^2 &= -N C_F g^2 |\Delta T_{q\bar{q}}^{(1)}|^2 \\ |\Delta T_{q\bar{q}}^{(1)}|^2 &= \left[\left\{ \frac{4 s Q^2 + 2 t^2 + 2 u^2}{t u} - \varepsilon \frac{(t+u)^2}{t u} \right\} \left(1 - \frac{\varepsilon}{2}\right) \right. \\ &\quad \left. - 4 \varepsilon + p_1^2 \frac{Q^2}{t^2} + p_2^2 \frac{Q^2}{u^2} \right], \\ K_{q\bar{q}} &= \frac{1}{N^2}, \\ q(\bar{q})(p_1) + g(p_2) &\rightarrow q(\bar{q})(k_1) + \gamma^*(q), \end{aligned} \quad (2.25)$$

$$\begin{aligned}
|\Delta M_{gg \rightarrow q \gamma^*}^{(1)}|^2 &= (N^2 - 1) T_f g^2 |\Delta T_{q\bar{q}}^{(1)}|^2 \\
|\Delta T_{q\bar{q}}^{(1)}|^2 &= \left[4 \frac{Q^2}{t} - 4 \frac{Q^2}{s} + 2 \frac{t}{s} - 2 \frac{s}{t} \right. \\
&\quad \left. + \varepsilon \left\{ 2 - 2 \frac{Q^2}{t} - 2 \frac{Q^2}{s} + \frac{t}{s} + \frac{s}{t} \right\} + p_2^2 \frac{2sQ^2 - 4Q^4}{st^2} \right], \\
K_{qg} &= \frac{1}{N(N^2 - 1)}, \tag{2.26}
\end{aligned}$$

$$q(\bar{q})(p_1) + g(p_2) \rightarrow q(\bar{q})(k_1) + H(q),$$

$$\begin{aligned}
|\Delta M_{gq \rightarrow q H}^{(1)}|^2 &= \frac{1}{4} N C_F g^2 \left[\frac{s^2 - t^2}{u} - p_1^2 \frac{Q^4}{u^2} \right], \\
K_{gq} &= \frac{1}{N(N^2 - 1)}, \tag{2.27}
\end{aligned}$$

$$g(p_1) + g(p_2) \rightarrow g(k_1) + H(q),$$

$$\begin{aligned}
|\Delta M_{gg \rightarrow g H}^{(1)}|^2 &= \frac{1}{4} N (N^2 - 1) g^2 \left[\frac{2s(s - Q^2) + 4Q^4}{t} + \frac{2s(s - Q^2) + 4Q^4}{u} \right. \\
&\quad \left. + \frac{2s^3}{tu} + \frac{3(s - Q^2)^2}{s} + \frac{t^2 + u^2}{s} \right. \\
&\quad \left. + p_1^2 \frac{3sQ^4 - 4Q^6}{st^2} + p_2^2 \frac{3sQ^4 - 4Q^6}{su^2} \right], \\
K_{gg} &= \frac{1}{(N^2 - 1)^2}. \tag{2.28}
\end{aligned}$$

Here g represents the strong coupling constant and the colour factors are given by

$$C_A = N, \quad C_F = \frac{N^2 - 1}{2N}, \quad T_f = \frac{1}{2}. \tag{2.29}$$

Notice that one has to put $p_i^2 = 0$ in the equations above if the matrix elements are understood to be used in the RSN scheme where the quarks are massless and the phase space integrals are evaluated in n dimensions. In the case of the off-shell regularization method one has to put $\varepsilon = 0$. Also we have neglected higher powers in p_i^2 since they do not contribute to the structure function in the limit $p_i^2 \rightarrow 0$. Further the off-shell matrix elements are gauge dependent and we have taken $l^\mu = l^\nu = 0$ for the polarization sum in Eq. (2.19) (Feynman gauge). In the case of the on-shell mass assignment we obtain

$$|\Delta M_{q\bar{q} \rightarrow g \gamma^*}^{(1)}|^2 = -N C_F g^2 \left[\frac{4sQ^2 + 2t^2 + 2u^2}{(t-m^2)(u-m^2)} + 4m^2 \left\{ \frac{sQ^2 - s^2 - Q^4}{s(t-m^2)^2} + \frac{sQ^2 - s^2 - Q^4}{s(u-m^2)^2} \right\} \right], \quad (2.30)$$

$$|\Delta M_{gg \rightarrow q \gamma^*}^{(1)}|^2 = (N^2 - 1) T_f g^2 \left[\frac{4Q^2 - 2s}{t-m^2} - \frac{4Q^2 - 2t}{s-m^2} - m^2 \frac{4Q^2}{(t-m^2)^2} \right], \quad (2.31)$$

$$|\Delta M_{gq \rightarrow q H}^{(1)}|^2 = \frac{1}{4} N C_F g^2 \left[\frac{s^2 - t^2}{u-m^2} \right]. \quad (2.32)$$

Notice that we have omitted the on-shell matrix element $|\Delta M_{gg}^{\text{on}(1)}|^2$ because the gluon is massless so there is no regulator mass for the collinear divergences when we integrate over the final state momenta.

Let us first start with the computation of the structure functions in the off-shell and on-shell mass assignments because they immediately lead to the correct coefficient functions in the $\overline{\text{MS}}$ -scheme. Integration over the final state momenta k_1 and q provides us with the following results. For the off-shell mass assignment we get

$$\Delta \hat{W}_{q\bar{q}}^{\text{off}(1)} = -a_s \frac{1}{N} C_F \left[\left\{ 4 \left(\frac{1}{1-x} \right)_+ - 2 - 2x \right\} \left\{ \ln \frac{Q^2}{-p_1^2} + \ln \frac{Q^2}{-p_2^2} \right\} \right]$$

$$\begin{aligned}
& +8 \left(\frac{\ln(1-x)}{1-x} \right)_+ - 4(1+x) \ln(1-x) - \frac{8(1+x^2)}{1-x} \ln x \\
& - 8 + 4x \Big], \tag{2.33}
\end{aligned}$$

$$\begin{aligned}
\Delta \hat{W}_{gg}^{\text{off}(1)} &= -a_s \frac{1}{N} T_f \left[\left\{ 4x - 2 \right\} \left\{ \ln \frac{Q^2}{-p_2^2} + \ln(1-x) - 2 \ln x \right\} \right. \\
& \left. + (1-x)(5+3x) - 2 \right], \tag{2.34}
\end{aligned}$$

$$\begin{aligned}
\Delta \hat{W}_{gq}^{\text{off}(1)} &= -a_s \frac{1}{N^2 - 1} C_F \left[\left\{ 4 - 2x \right\} \left\{ \ln \frac{Q^2}{-p_1^2} + \ln(1-x) - 2 \ln x \right\} \right. \\
& \left. + \frac{3}{x}(1-x)^2 - 2 \right], \tag{2.35}
\end{aligned}$$

$$\begin{aligned}
\Delta \hat{W}_{gq}^{\text{off}(1)} &= -a_s \frac{1}{N^2 - 1} C_A \left[\left\{ 4 \left(\frac{1}{1-x} \right)_+ + 4 - 8x \right\} \left\{ \ln \frac{Q^2}{-p_1^2} + \ln \frac{Q^2}{-p_2^2} \right\} \right. \\
& + 8 \left(\frac{\ln(1-x)}{1-x} \right)_+ + (8 - 16x) \ln(1-x) - \left(\frac{16}{1-x} + 16 \right. \\
& \left. \left. - 32x \right) \ln x + \frac{22}{3x} (1-x)^3 - 12 + 16x \Big], \tag{2.36}
\end{aligned}$$

where we have introduced the shorthand notation

$$a_s = \frac{\alpha_s}{4\pi} = \frac{g^2}{(4\pi)^2}. \tag{2.37}$$

Notice that we have omitted the soft-plus-virtual gluon corrections in Eq. (2.33) and Eq. (2.36) which are proportional to $\delta(1-x)$. As was pointed out in [23] these terms cannot be correctly computed using the off-shell assignment according to Eq. (2.18). In the case of the on-shell mass assignment

we can compute the latter correction and we obtain

$$\begin{aligned} \Delta \hat{W}_{q\bar{q}}^{\text{on}(1)} &= -a_s \frac{1}{N} C_F \left[\left\{ 8 \left(\frac{1}{1-x} \right)_+ - 4 - 4x \right\} \ln \frac{Q^2}{m^2} \right. \\ &\quad \left. - \frac{4(1+x^2)}{1-x} \ln x - 8 \left(\frac{1}{1-x} \right)_+ - 4 + 12x \right. \\ &\quad \left. + \delta(1-x) \left\{ 6 \ln \frac{Q^2}{m^2} - 8 + 8\zeta(2) \right\} \right], \end{aligned} \quad (2.38)$$

$$\begin{aligned} \Delta \hat{W}_{qg}^{\text{on}(1)} &= -a_s \frac{1}{N} T_f \left[\left\{ 4x - 2 \right\} \left\{ \ln \frac{Q^2}{m^2} + 2 \ln(1-x) - \ln x \right\} \right. \\ &\quad \left. + (1-x)(5+3x) \right], \end{aligned} \quad (2.39)$$

$$\begin{aligned} \Delta \hat{W}_{gq}^{\text{on}(1)} &= -a_s \frac{1}{N^2 - 1} C_F \left[\left\{ 4 - 2x \right\} \left\{ \ln \frac{Q^2}{m^2} + 2 \ln(1-x) - 3 \ln x \right\} \right. \\ &\quad \left. + \frac{3}{x} (1-x)^2 \right]. \end{aligned} \quad (2.40)$$

Eqs. (2.34) and (2.39) are in agreement with [36]. A comparison with the unpolarized structure functions $W_{q\bar{q}}^{(0)}$ and $\hat{W}_{q\bar{q}}^{(1)}$ as computed for instance in [23] reveals the following relations

$$\begin{aligned} \Delta W_{q\bar{q}}^{(0)} &= -W_{q\bar{q}}^{(0)}, & \Delta \hat{W}_{q\bar{q}}^{\text{off}(1)} &= -\hat{W}_{q\bar{q}}^{\text{off}(1)}, \\ \Delta \hat{W}_{q\bar{q}}^{\text{on}(1)} &= -\hat{W}_{q\bar{q}}^{\text{on}(1)} + a_s \frac{1}{N} C_F [8(1-x)]. \end{aligned} \quad (2.41)$$

The last term is due to chiral symmetry breaking since the quark has a mass $m \neq 0$.

We will now present the coefficient functions following from mass factorization denoted by

$$\Delta \hat{W}_{ij} = \sum_{k,l=q,g} \Delta \Gamma_{ki} \Delta \Gamma_{lj} \Delta W_{kl}. \quad (2.42)$$

In the formula above all collinear divergences are absorbed by the kernels $\Delta\Gamma_{kl}$ which depend on $\ln \mu^2/p_i^2$, $\ln \mu^2/m^2$ or $1/\varepsilon$ depending on the regularization method used. Here μ represents the factorization scale which also enters the finite DY coefficient functions ΔW_{kl} . In NLO the latter are given by

$$\begin{aligned}
\Delta W_{qq}^{(1)} &= \Delta \hat{W}_{qq}^{(1)} - 2 \Delta \Gamma_{qq}^{(1)}, \\
\Delta W_{qg}^{(1)} &= \Delta \hat{W}_{qg}^{(1)} - \Delta \Gamma_{qg}^{(1)}, \\
\Delta W_{gq}^{(1)} &= \Delta \hat{W}_{gq}^{(1)} - \Delta \Gamma_{gq}^{(1)}, \\
\Delta W_{gg}^{(1)} &= \Delta \hat{W}_{gg}^{(1)} - 2 \Delta \Gamma_{gg}^{(1)}.
\end{aligned} \tag{2.43}$$

In the case of the off- and on-shell regularization the kernels are given by the operator matrix elements as follows

$$\Delta\Gamma_{qq} = \Delta A_{qq}, \quad \Delta\Gamma_{qg} = \frac{1}{2} \Delta A_{qg}, \quad \Delta\Gamma_{gq} = \Delta A_{gq}, \quad \Delta\Gamma_{gg} = \Delta A_{gg}. \tag{2.44}$$

For the off-shell mass assignment the latter can be found in [19], [21] and they are given by

$$\begin{aligned}
\Delta A_{iq} &= \Delta A_{iq}^{\text{PHYS}} + \Delta A_{iq}^{\text{EOM}}, \\
\Delta A_{ig} &= \Delta A_{ig}^{\text{PHYS}}, \quad i = q, g.
\end{aligned} \tag{2.45}$$

The term $\Delta A_{iq}^{\text{EOM}}$ is characteristic of the off-shell mass assignment and it vanishes when the equations of motions (EOM) are applied to the external quark indicated by the momentum p so that it does not show up in the on-shell case. In the Feynman gauge and renormalized in the $\overline{\text{MS}}$ -scheme they read

$$\begin{aligned}
\Delta A_{qq}^{\text{PHYS,off}} &= \delta(1-x) + a_s C_F \left[\left\{ 4 \left(\frac{1}{1-x} \right)_+ - 2 - 2x \right\} \ln \frac{\mu^2}{-p^2} \right. \\
&\quad \left. - 4 \left(\frac{\ln(1-x)}{1-x} \right)_+ + 2(1+x) \ln(1-x) - \frac{2(1+x^2)}{1-x} \ln x \right]
\end{aligned}$$

$$-4 + 6x + \delta(1-x) \left\{ 3 \ln \frac{\mu^2}{-p^2} + 7 - 4\zeta(2) \right\}, \quad (2.46)$$

$$\Delta A_{qq}^{\text{EOM,off}} = a_s C_F \left[-4x \right], \quad (2.47)$$

$$\Delta A_{gg}^{\text{PHYS,off}} = a_s T_f \left[\left\{ 8x - 4 \right\} \left\{ \ln \frac{\mu^2}{-p^2} - \ln(1-x) - \ln x \right\} - 4 \right], \quad (2.48)$$

$$\Delta A_{gq}^{\text{PHYS,off}} = a_s C_F \left[\left\{ 4 - 2x \right\} \left\{ \ln \frac{\mu^2}{-p^2} - \ln(1-x) - \ln x \right\} - 2 \right], \quad (2.49)$$

$$\Delta A_{gq}^{\text{EOM,off}} = a_s C_F \left[4(1-x) \right], \quad (2.50)$$

$$\begin{aligned} \Delta A_{gg}^{\text{PHYS,off}} = & \delta(1-x) + a_s C_A \left[\left\{ 4 \left(\frac{1}{1-x} \right)_+ + 4 - 8x \right\} \ln \frac{\mu^2}{-p^2} \right. \\ & - 4 \left(\frac{\ln(1-x)}{1-x} \right)_+ + (-4 + 8x) \ln(1-x) - \left(\frac{4}{1-x} \right. \\ & \left. \left. + 4 - 8x \right) \ln x + 2 + \delta(1-x) \left\{ \frac{11}{3} \ln \frac{\mu^2}{-p^2} + \frac{67}{9} - 4\zeta(2) \right\} \right] \\ & + a_s n_f T_f \delta(1-x) \left[-\frac{4}{3} \ln \frac{\mu^2}{-p^2} - \frac{20}{9} \right]. \end{aligned} \quad (2.51)$$

The results above are calculated using the HVBM prescription according to Eq. (2.16). In this case the renormalization constants become equal to

$$Z_{ij}^{\text{HVBM}} = \delta_{ij} \delta(1-x) + a_s \left[\frac{1}{2} \Delta P_{ij}^{(0)} \left(\frac{2}{\varepsilon} + \gamma_E - \ln 4\pi \right) \right] \quad i, j = q, g, \quad (2.52)$$

where $\Delta P_{ij}^{(0)}$ are the lowest order polarized splitting functions (see e.g. [19], [20]) given by

$$\Delta P_{gq}^{(0)} = T_f [16x - 8],$$

$$\begin{aligned}
\Delta P_{gq}^{(0)} &= C_F [8 - 4x], \\
\Delta P_{gg}^{(0)} &= C_A \left[8 \left(\frac{1}{(1-x)} \right)_+ + 8 - 16x + \frac{22}{3} \delta(1-x) \right] \\
&\quad - \frac{8}{3} n_f T_f \delta(1-x). \tag{2.53}
\end{aligned}$$

However there is one exception in the case of Z_{qq} . For the HVBM prescription the latter is given by

$$\begin{aligned}
Z_{qq}^{\text{HVBM}} &= \delta(1-x) + a_s \left[\frac{1}{2} \Delta P_{qq}^{(0)} \left(\frac{2}{\varepsilon} + \gamma_E - \ln 4\pi \right) \right] \\
&\quad - a_s C_F [8(1-x)], \\
\Delta P_{qq}^{(0)} &= C_F \left[8 \left(\frac{1}{(1-x)} \right)_+ - 4 - 4x + 6\delta(1-x) \right]. \tag{2.54}
\end{aligned}$$

The last term in Z_{qq}^{HVBM} is the evanescent counter term which is necessary to ensure that the non-singlet axial vector current does not get renormalized. This implies that the first moment of $\Delta A_{qq}^{\text{PHYS}}$ must be unity in all orders of perturbation theory. Notice that in higher order the evanescent counter term even becomes infinite (see [18], [21]).³ Using the same counter terms as in Eqs. (2.52), (2.54) one obtains the following expressions for the operator matrix elements in the on-shell mass assignment. Using the notation in Eq. (2.45) the operator matrix elements $\Delta A_{ij}^{\text{PHYS}}$ become equal to

$$\begin{aligned}
\Delta A_{qq}^{\text{on}} &= \delta(1-x) + a_s C_F \left[\left\{ 4 \left(\frac{1}{1-x} \right)_+ - 2 - 2x \right\} \ln \frac{\mu^2}{m^2} \right. \\
&\quad \left. - 8 \left(\frac{\ln(1-x)}{1-x} \right)_+ + 4(1+x) \ln(1-x) - 4 \left(\frac{1}{1-x} \right)_+ \right. \\
&\quad \left. - 2 + 6x + \delta(1-x) \left\{ 3 \ln \frac{\mu^2}{m^2} + 4 \right\} \right], \tag{2.55}
\end{aligned}$$

³It appears that in the case of the naive γ_5 -matrix prescription, where this matrix anti-commutes with the other γ -matrices in n dimensions, an evanescent counter term is not necessary in the non-singlet case.

$$\Delta A_{gg}^{\text{on}} = a_s T_f \left[\left\{ 8x - 4 \right\} \ln \frac{\mu^2}{m^2} \right], \quad (2.56)$$

$$\Delta A_{gq}^{\text{on}} = a_s C_F \left[\left\{ 4 - 2x \right\} \left\{ \ln \frac{\mu^2}{m^2} - 2 \ln x \right\} + 4(1 - x) \right], \quad (2.57)$$

and $\Delta A_{iq}^{\text{EOM}} = 0$. Notice that the first moment of $\Delta A_{qq}^{\text{on}}$ in Eq. (2.55) is still not equal to unity even after subtraction of the evanescent counter term. This is because the non-singlet axial vector current is not conserved for massive quarks and therefore has to undergo a finite renormalization. This additional term, which is equal to $a_s C_F 4(1 - x)$, will compensate the last term in Eq. (2.41) while computing the difference in Eq. (2.43). After mass factorization one obtains the same coefficient functions irrespective whether the off-shell or the on-shell regularization is used. The results are

$$\begin{aligned} \Delta W_{q\bar{q}}^{(1)} &= -a_s \frac{1}{N} C_F \left[\left\{ 8 \left(\frac{1}{1-x} \right)_+ - 4 - 4x \right\} \ln \frac{Q^2}{\mu^2} \right. \\ &\quad \left. + 16 \left(\frac{\ln(1-x)}{1-x} \right)_+ - 8(1+x) \ln(1-x) - \frac{4(1+x^2)}{1-x} \ln x \right. \\ &\quad \left. + \delta(1-x) \left\{ 6 \ln \frac{Q^2}{\mu^2} - 16 + 8\zeta(2) \right\} \right], \quad (2.58) \end{aligned}$$

$$\begin{aligned} \Delta W_{gg}^{(1)} &= -a_s \frac{1}{N} T_f \left[\left\{ 4x - 2 \right\} \left\{ \ln \frac{Q^2}{\mu^2} + 2 \ln(1-x) - \ln x \right\} \right. \\ &\quad \left. + (1-x)(5 + 3x) \right], \quad (2.59) \end{aligned}$$

$$\begin{aligned} \Delta W_{gq}^{(1)} &= -a_s \frac{1}{N^2 - 1} C_F \left[\left\{ 4 - 2x \right\} \left\{ \ln \frac{Q^2}{\mu^2} + 2 \ln(1-x) - \ln x \right\} \right. \\ &\quad \left. + \frac{3}{x} (1-x)^2 - 4(1-x) \right], \quad (2.60) \end{aligned}$$

$$\begin{aligned}
\Delta W_{gg}^{(1)} &= -a_s \frac{1}{N^2 - 1} C_A \left[\left\{ 8 \left(\frac{1}{1-x} \right)_+ + 8 - 16x \right\} \ln \frac{Q^2}{\mu^2} \right. \\
&\quad + 16 \left(\frac{\ln(1-x)}{1-x} \right)_+ + (16 - 32x) \ln(1-x) \\
&\quad - \left(\frac{8}{1-x} + 8 - 16x \right) \ln x + \frac{22}{3x} (1-x)^3 - 16(1-x) \\
&\quad \left. + \delta(1-x) \left\{ \frac{22}{3} + 8\zeta(2) \right\} \right]. \tag{2.61}
\end{aligned}$$

Notice that the coefficient of the $\delta(1-x)$ term in Eq. (2.58) can only be obtained from the on-shell scheme. The latter scheme could not be applied to the process $g + g \rightarrow g + H$ in Eq. (2.28) so that the $\delta(1-x)$ -term in Eq. (2.61) can only be inferred from n -dimensional regularization as HVBM or RSN. Furthermore from Eq. (2.58) one derives

$$\Delta W_{q\bar{q}}^{(1)} = -W_{q\bar{q}}^{(1)}. \tag{2.62}$$

This relation, which only holds for coefficient functions, has to be satisfied irrespective which regularization scheme is chosen.

Now we want to compute the coefficients above using the RSN approach presented in Eq. (2.19) and determine the corresponding evanescent counter terms. The DY partonic structure functions are given by

$$\begin{aligned}
\Delta \hat{W}_{q\bar{q}}^{\text{RSN},(1)} &= \Delta W_{q\bar{q}}^{(1)} - a_s \frac{1}{N} \left[\Delta P_{q\bar{q}}^{(0)} \left(\frac{2}{\varepsilon} + \gamma_E - \ln 4\pi \right) \right] \\
&\quad + a_s \frac{1}{N} C_F [8(1-x)], \tag{2.63}
\end{aligned}$$

$$\begin{aligned}
\Delta \hat{W}_{gg}^{\text{RSN},(1)} &= \Delta W_{gg}^{(1)} - a_s \frac{1}{N} \left[\frac{1}{4} \Delta P_{gg}^{(0)} \left(\frac{2}{\varepsilon} + \gamma_E - \ln 4\pi \right) \right] \\
&\quad + a_s \frac{1}{N} T_f [4(1-x)], \tag{2.64}
\end{aligned}$$

$$\Delta \hat{W}_{gq}^{\text{RSN},(1)} = \Delta W_{gq}^{(1)} - a_s \frac{1}{N^2 - 1} \left[\frac{1}{2} \Delta P_{gq}^{(0)} \left(\frac{2}{\varepsilon} + \gamma_E - \ln 4\pi \right) \right]$$

$$-a_s \frac{1}{N^2 - 1} C_F [4(1-x)], \quad (2.65)$$

$$\begin{aligned} \Delta \hat{W}_{gg}^{\text{RSN},(1)} &= \Delta W_{gg}^{(1)} - a_s \frac{1}{N^2 - 1} \left[\Delta P_{gg}^{(0)} \left(\frac{2}{\varepsilon} + \gamma_E - \ln 4\pi \right) \right] \\ &\quad - a_s \frac{1}{N^2 - 1} C_A [16(1-x)]. \end{aligned} \quad (2.66)$$

This scheme violates the relation in Eq. (2.62) in a similar way as the on-shell result in Eq. (2.41). This is because the n -dimensional extension of the γ_5 -matrix breaks the chiral symmetry. However this is unphysical because the quarks are still massless. The kernels for the RSN prescription follow from the requirement that the RSN-scheme must lead to the same coefficient functions as the four dimensional regularization methods. From mass factorization (see Eq. (2.43)) and the coefficient functions presented in Eqs. (2.58)-(2.61) we infer the kernels

$$\begin{aligned} \Delta \Gamma_{qq}^{\text{RSN}} &= \delta(1-x) + a_s \left[\frac{1}{2} \Delta P_{qq}^{(0)} \left(\frac{2}{\varepsilon} + \gamma_E - \ln 4\pi \right) \right] \\ &\quad - a_s C_F [4(1-x)], \end{aligned} \quad (2.67)$$

$$\begin{aligned} \Delta \Gamma_{gg}^{\text{RSN}} &= a_s \left[\frac{1}{4} \Delta P_{gg}^{(0)} \left(\frac{2}{\varepsilon} + \gamma_E - \ln 4\pi \right) \right] \\ &\quad - a_s T_f [4(1-x)], \end{aligned} \quad (2.68)$$

$$\begin{aligned} \Delta \Gamma_{gq}^{\text{RSN}} &= a_s \left[\frac{1}{2} \Delta P_{gq}^{(0)} \left(\frac{2}{\varepsilon} + \gamma_E - \ln 4\pi \right) \right] \\ &\quad + a_s C_F [4(1-x)], \end{aligned} \quad (2.69)$$

$$\begin{aligned} \Delta \Gamma_{gg}^{\text{RSN}} &= \delta(1-x) + a_s \left[\frac{1}{2} \Delta P_{gg}^{(0)} \left(\frac{2}{\varepsilon} + \gamma_E - \ln 4\pi \right) \right] \\ &\quad + a_s C_A [8(1-x)], \end{aligned} \quad (2.70)$$

where the additional terms are characteristic of the RSN-scheme.

Finally we want to show that the prescription given in Eq. (2.16) leads to the same results as the conventional HVBM approach in [16] and [17]. A straightforward calculation gives

$$\begin{aligned} \Delta \hat{W}_{q\bar{q}}^{\text{HVBM},(1)} &= \Delta W_{q\bar{q}}^{(1)} - a_s \frac{1}{N} \left[\Delta P_{qq}^{(0)} \left(\frac{2}{\varepsilon} + \gamma_E - \ln 4\pi \right) \right] \\ &\quad + a_s \frac{1}{N} C_F [16(1-x)], \end{aligned} \quad (2.71)$$

$$\Delta \hat{W}_{qg}^{\text{HVBM},(1)} = \Delta W_{qg}^{(1)} - a_s \frac{1}{N} \left[\frac{1}{4} \Delta P_{qg}^{(0)} \left(\frac{2}{\varepsilon} + \gamma_E - \ln 4\pi \right) \right], \quad (2.72)$$

$$\Delta \hat{W}_{gq}^{\text{HVBM},(1)} = \Delta W_{gq}^{(1)} - a_s \frac{1}{N^2 - 1} \left[\frac{1}{2} \Delta P_{qg}^{(0)} \left(\frac{2}{\varepsilon} + \gamma_E - \ln 4\pi \right) \right], \quad (2.73)$$

$$\Delta \hat{W}_{gg}^{\text{HVBM},(1)} = \Delta W_{gg}^{(1)} - a_s \frac{1}{N^2 - 1} \left[\Delta P_{gg}^{(0)} \left(\frac{2}{\varepsilon} + \gamma_E - \ln 4\pi \right) \right]. \quad (2.74)$$

The results in Eqs. (2.71) and (2.72) agree with those in [6] which were obtained by the conventional HVBM approach. The kernels for the HVBM prescription are obtained according to the same requirement as used for the RSN-approach above Eq. (2.67) and they read

$$\begin{aligned} \Delta \Gamma_{q\bar{q}}^{\text{HVBM}} &= \delta(1-x) + a_s \left[\frac{1}{2} \Delta P_{qq}^{(0)} \left(\frac{2}{\varepsilon} + \gamma_E - \ln 4\pi \right) \right] \\ &\quad - a_s C_F [8(1-x)], \end{aligned} \quad (2.75)$$

$$\Delta \Gamma_{qg}^{\text{HVBM}} = a_s \left[\frac{1}{4} \Delta P_{qg}^{(0)} \left(\frac{2}{\varepsilon} + \gamma_E - \ln 4\pi \right) \right], \quad (2.76)$$

$$\Delta \Gamma_{gq}^{\text{HVBM}} = a_s \left[\frac{1}{2} \Delta P_{qg}^{(0)} \left(\frac{2}{\varepsilon} + \gamma_E - \ln 4\pi \right) \right], \quad (2.77)$$

$$\Delta \Gamma_{gg}^{\text{HVBM}} = \delta(1-x) + a_s \left[\frac{1}{2} \Delta P_{gg}^{(0)} \left(\frac{2}{\varepsilon} + \gamma_E - \ln 4\pi \right) \right]. \quad (2.78)$$

As in the case of unpolarized quantities the kernels above are equal to the operator renormalization constants in Eqs. (2.52), (2.53), except that

$\Delta\Gamma_{gg}^{\text{HVBM}} = 1/2 \Delta Z_{gg}^{\text{HVBM}}$ (see also Eq. (2.44)), provided the same γ_5 -matrix prescription is used for ultraviolet and collinear divergences. Further notice that RSN and HVBM schemes only affect the regular part of the kernels and do not alter the singular part represented by $\delta(1-x)$.

Summarizing the results obtained in this section we have introduced a new scheme, called RSN, which is designed to regularize the hard gluon contributions to the double differential structure functions in Eq. (2.4) when the latter are computed in NLO. For that purpose we calculated the evanescent counter terms by the requirement that in the $\overline{\text{MS}}$ scheme one should obtain the same coefficient functions as obtained by four dimensional regularization methods. One of the most important results is the relation between the polarized and unpolarized structure functions in Eq. (2.62) which has to be satisfied irrespective of the prescription used for the γ_5 -matrix. That this relation has to emerge from the calculations can be simply inferred from the off-shell regularization technique (see the result for $W_{q\bar{q}}$ in Eq. (2.41)). In four dimensions the two γ_5 -matrices in the non-singlet part of the matrix element in Eq. (2.9) can be brought together since they are present in the same trace so that they yield unity. In this way the matrix element becomes the same as for unpolarized reactions.

3 NLO corrections to polarized lepton-pair production

After having specified the RSN-prescription for the γ_5 matrix and the Levi-Civita tensor in the previous section we present the NLO corrections to the quantity

$$\begin{aligned}
s \frac{d^2 \Delta \hat{W}_{a_1 a_2}^{(1)}}{d t d u} &= K_{a_1 a_2} \frac{S_\varepsilon}{(4\pi)^2 \Gamma(1 + \varepsilon/2)} \left(\frac{t u}{Q^2 s} \right)^{\varepsilon/2} \delta(s + t + u - Q^2) \\
&\times |\Delta M_{a_1 a_2 \rightarrow b_1 \gamma^*}^{(1)}|^2, \quad \text{with } n = 4 + \varepsilon. \quad (3.1)
\end{aligned}$$

Here $\Gamma(x)$ denotes the gamma-function and the spherical factor S_ε is defined by

$$S_\varepsilon = \exp\left(\frac{\varepsilon}{2}(\gamma_E - \ln 4\pi)\right). \quad (3.2)$$

Notice that the expression in Eq. (3.1) holds for the Born reactions in Eq. (2.25), (2.26) as well as for the virtual corrections presented below. The calculation proceeds in the same way as e.g. done in the case of unpolarized processes like heavy flavour production [37] or Higgs production [26]. Starting with the virtual contributions we compute the one-loop corrections to the reactions in Eqs. (2.25), (2.26). The Feynman graphs can be found in Fig 5 of [30]. First we perform tensorial reduction of the Feynman integrals into scalar integrals following the procedure in [34], [35]. The scalar integrals can be found in Appendix D of [38] and we use n -dimensional regularization for the ultraviolet, infrared and collinear divergences. Finally we contract the Levi-Civita tensors in four dimensions. The results which hold in the HVBM- as well as RSN-schemes are given by

$$\begin{aligned}
s \frac{d^2 \Delta \hat{W}_{q\bar{q}}^V}{d t d u} &= \delta(s + t + u - Q^2) S_\varepsilon^2 a_s^2 \frac{1}{N} \\
&\times \left[C_F(C_F - C_A/2) \left\{ \frac{8}{\varepsilon^2} + \left(8 \ln \frac{-t}{\mu^2} - 6 \right) \frac{1}{\varepsilon} \right. \right. \\
&\quad \left. \left. - 4 \text{Li}_2\left(\frac{s - Q^2}{s}\right) - 4 \text{Li}_2\left(\frac{t}{Q^2}\right) + 2 \ln \frac{-t}{\mu^2} \ln \frac{-u}{\mu^2} \right. \right.
\end{aligned}$$

$$\begin{aligned}
& +4 \ln \frac{-t}{\mu^2} \ln \frac{s}{\mu^2} - 2 \ln^2 \frac{s}{\mu^2} + 2 \ln^2 \left(\frac{t - Q^2}{t} \right) \\
& - 2 \ln^2 \left(\frac{Q^2 - t}{Q^2} \right) - 6 \ln \frac{-t}{\mu^2} + 3 \ln \frac{s}{Q^2} - 8 \zeta(2) + 8 \\
& + (t \Leftrightarrow u) \left. \right\} \times |\Delta T_{q\bar{q}}^{(1)}|^2 \\
& + C_A C_F \left\{ \frac{8}{\varepsilon^2} + \left(12 \ln \frac{-t}{\mu^2} - 4 \ln \frac{s}{\mu^2} - 3 \right) \frac{1}{\varepsilon} - 2 \text{Li}_2 \left(\frac{t}{Q^2} \right) \right. \\
& + 5 \ln \frac{-t}{\mu^2} \ln \frac{-u}{\mu^2} - 6 \ln \frac{-t}{\mu^2} \ln \frac{s}{\mu^2} + 4 \ln^2 \frac{-t}{\mu^2} + \ln^2 \frac{s}{\mu^2} \\
& + \ln^2 \left(\frac{t - Q^2}{t} \right) - \ln^2 \left(\frac{Q^2 - t}{Q^2} \right) - 3 \ln \frac{-t}{\mu^2} + \frac{3}{2} \ln \frac{s}{Q^2} \\
& \left. - 7 \zeta(2) + 4 + (t \Leftrightarrow u) \right\} |\Delta T_{q\bar{q}}^{(1)}|^2 \\
& + C_F (C_F - C_A/2) \left\{ \frac{16s + 8t}{u} \left(\text{Li}_2 \left(\frac{t}{Q^2} \right) + \text{Li}_2 \left(\frac{s - Q^2}{s} \right) \right) \right. \\
& + \frac{1}{2} \ln^2 \frac{-t}{s} - \frac{1}{2} \ln^2 \left(\frac{t - Q^2}{t} \right) + \frac{1}{2} \ln^2 \left(\frac{Q^2 - t}{Q^2} \right) \left. \right) \\
& + \frac{8s(s - 2Q^2)}{(s - Q^2)^2} \ln \frac{s}{Q^2} + \left(\frac{4tu}{(Q^2 - t)^2} - \frac{8(t - 2u)}{Q^2 - t} - 16 \right) \\
& \times \ln \frac{-t}{Q^2} + \frac{4(s + u)}{t} + \frac{8s}{s - Q^2} + \frac{4u}{Q^2 - t} - 4 + (t \Leftrightarrow u) \left. \right\} \\
& + C_A C_F \left\{ \left(\frac{2tu}{(Q^2 - t)^2} + \frac{8(u - t)}{Q^2 - t} - 8 \right) \ln \frac{-t}{Q^2} - \frac{2(s + u)}{t} \right.
\end{aligned}$$

$$\left. + \frac{2u}{Q^2 - t} - 2 + (t \Leftrightarrow u) \right\} \Big]. \quad (3.3)$$

Apart from an overall minus sign the above result agrees with the unpolarized virtual contribution in [11]. Note that ε terms in $|\Delta T_{q\bar{q}}^{(1)}|^2$ (see Eq. (2.25)) differ from those in the unpolarized case, denoted by $|T_{q\bar{q}}^{(1)}|^2$, which causes the breakdown of the relation in Eq. (2.62). Also we find

$$\begin{aligned} s \frac{d^2 \Delta \hat{W}_{qg}^V}{d t d u} &= \delta(s + t + u - Q^2) S_\varepsilon^2 a_s^2 \frac{1}{N} \\ &\times \left[C_F \left\{ -\frac{8}{\varepsilon^2} + \left(-4 \ln \frac{-t}{\mu^2} - 8 \ln \frac{-u}{\mu^2} + 4 \ln \frac{s}{\mu^2} + 6 \right) \frac{1}{\varepsilon} \right. \right. \\ &+ 2 \text{Li}_2 \left(\frac{t}{Q^2} \right) + 2 \text{Li}_2 \left(\frac{u}{Q^2} \right) - 6 \ln \frac{-t}{\mu^2} \ln \frac{-u}{\mu^2} \\ &+ 2 \ln \frac{-t}{\mu^2} \ln \frac{s}{\mu^2} + 4 \ln \frac{-u}{\mu^2} \ln \frac{s}{\mu^2} - 3 \ln^2 \frac{-u}{\mu^2} - \ln^2 \frac{s}{\mu^2} \\ &- \ln^2 \left(\frac{t - Q^2}{t} \right) - \ln^2 \left(\frac{u - Q^2}{u} \right) + \ln^2 \left(\frac{Q^2 - t}{Q^2} \right) \\ &\left. \left. + \ln^2 \left(\frac{Q^2 - u}{Q^2} \right) + 3 \ln \frac{tu}{s\mu^2} + 3 \ln \frac{Q^2}{\mu^2} + 12 \zeta(2) - 9 \right\} \right. \\ &\times |\Delta T_{qg}^{(1)}|^2 \\ &+ C_A \left\{ -\frac{4}{\varepsilon^2} - \left(4 \ln \frac{-t}{\mu^2} \right) \frac{1}{\varepsilon} + \text{Li}_2 \left(\frac{s - Q^2}{s} \right) - \text{Li}_2 \left(\frac{u}{Q^2} \right) \right. \\ &- 2 \ln^2 \frac{-t}{\mu^2} + \frac{1}{2} \ln^2 \frac{u}{s} + \frac{1}{2} \ln^2 \left(\frac{u - Q^2}{u} \right) \\ &\left. \left. - \frac{1}{2} \ln^2 \left(\frac{Q^2 - u}{Q^2} \right) - \zeta(2) + 1 \right\} |\Delta T_{qg}^{(1)}|^2 \end{aligned}$$

$$\begin{aligned}
& +C_F \left\{ \frac{4(t+2u)}{s} \left(-\text{Li}_2 \left(\frac{s-Q^2}{s} \right) + \text{Li}_2 \left(\frac{t}{Q^2} \right) \right. \right. \\
& - \ln \frac{-u}{\mu^2} \ln \frac{-t}{s} + \frac{1}{2} \ln^2 \frac{-t}{\mu^2} - \frac{1}{2} \ln^2 \frac{s}{\mu^2} - \frac{1}{2} \ln^2 \left(\frac{t-Q^2}{t} \right) \\
& + \frac{1}{2} \ln^2 \left(\frac{Q^2-t}{Q^2} \right) + 5\zeta(2) \left. \right) + \left(\frac{2su}{(s-Q^2)^2} - \frac{2(s+4u)}{s-Q^2} \right) \\
& \times \ln \frac{s}{Q^2} + \left(\frac{2st}{(Q^2-t)^2} + \frac{4(2s-t)}{Q^2-t} - 8 \right) \ln \frac{-t}{Q^2} - \frac{2u}{s} + \frac{2u}{t} \\
& + \frac{2s}{Q^2-t} - \frac{2u}{s-Q^2} - 2 \left. \right\} \\
& +C_A \left\{ \frac{2(t+2u)}{s} \left(\text{Li}_2 \left(\frac{s-Q^2}{s} \right) - \text{Li}_2 \left(\frac{t}{Q^2} \right) \right. \right. \\
& + \ln \frac{-u}{\mu^2} \ln \frac{-t}{s} - \frac{1}{2} \ln^2 \frac{-t}{\mu^2} + \frac{1}{2} \ln^2 \frac{s}{\mu^2} + \frac{1}{2} \ln^2 \left(\frac{t-Q^2}{t} \right) \\
& - \frac{1}{2} \ln^2 \left(\frac{Q^2-t}{Q^2} \right) - 5\zeta(2) \left. \right) - \frac{2s}{s-Q^2} \ln \frac{s}{Q^2} \\
& - \frac{2t}{Q^2-t} \ln \frac{-t}{Q^2} + \frac{2u}{s} - \frac{2u}{t} \left. \right\} . \tag{3.4}
\end{aligned}$$

Here the function $\text{Li}_2(x)$ in the expressions above denotes the di-logarithm which e.g. can be found in [39]. Next we compute all $2 \rightarrow 3$ -body processes which contribute to the structure function

$$\begin{aligned}
s \frac{d^2 \Delta \hat{W}_{a_1 a_2}^{(2)}}{d t d u} &= \frac{1}{2\pi} K_{a_1 a_2} \frac{S_\varepsilon^2}{(4\pi)^4 \Gamma(1+\varepsilon)} \left(\frac{t u - Q^2 s_4}{\mu^2 s} \right)^{\varepsilon/2} \left(\frac{s_4}{\mu^2} \right)^{\varepsilon/2} \\
&\times \overline{|\Delta M_{a_1 a_2 \rightarrow b_1 b_2 \gamma^*}^{(2)}|^2}, \\
&\text{with } s_4 = s + t + u - Q^2, \tag{3.5}
\end{aligned}$$

where $\overline{|\Delta M_{a_1 a_2 \rightarrow b_1 b_2 \gamma^*}^{(2)}|^2}$ is the second order matrix element integrated over the polar angle θ_1 and the azimuthal angle θ_2 so

$$\begin{aligned} & \overline{|\Delta M_{a_1 a_2 \rightarrow b_1 b_2 \gamma^*}^{(2)}|^2} \\ &= \int_0^\pi d\theta_1 (\sin \theta_1)^{1+\varepsilon} \int_0^\pi d\theta_2 (\sin \theta_2)^\varepsilon |\Delta M_{a_1 a_2 \rightarrow b_1 b_2 \gamma^*}^{(2)}(\theta_1, \theta_2)|^2 \\ &\equiv \int d\Omega_{n-1} |\Delta M_{a_1 a_2 \rightarrow b_1 b_2 \gamma^*}^{(2)}(\theta_1, \theta_2)|^2. \end{aligned} \quad (3.6)$$

The Feynman graphs for the $2 \rightarrow 3$ body parton subprocesses can be found in Figs. 6-9 in [30]. These reactions have been calculated using two different regularization methods for the collinear divergences. In n dimensions we use the RSN prescription mentioned in Eq. (2.19). In this case the collinear divergences in Eq. (3.6) manifest themselves as pole terms of the type $1/\varepsilon$. For $n = 4$ we adopted the off shell regularization method in Eq. (2.18) where the collinear divergences show up as logarithms $\ln s/p^2$. Notice that the off-shell regularization technique is gauge dependent and we have computed Eq. (3.6) in the Feynman gauge (see the comments below Eq. (2.29)). The gauge dependent terms will be cancelled after mass factorization via the operator matrix elements in Eqs. (2.45)-(2.50) which are computed in the same gauge. Decomposing the matrix element in Eq. (3.6) into colour factors one obtains the following results for the non-singlet $q\bar{q}$ and the singlet qg subprocesses

$$\begin{aligned} & q + \bar{q} \rightarrow g + g + \gamma^*, \\ \overline{|\Delta M_{q\bar{q} \rightarrow gg \gamma^*}^{(2)}|^2} &= g^4 e_q^2 \left[C_A C_F^2 \overline{|\Delta T_{q\bar{q}}^{(2)}|^2}_{C_F} + C_A^2 C_F \overline{|\Delta T_{q\bar{q}}^{(2)}|^2}_{C_A} \right], \end{aligned} \quad (3.7)$$

$$\begin{aligned} & q + g \rightarrow q + g + \gamma^*, \\ \overline{|\Delta M_{qg \rightarrow qg \gamma^*}^{(2)}|^2} &= g^4 e_q^2 \left[C_A C_F^2 \overline{|\Delta T_{qg}^{(2)}|^2}_{C_F} + C_A^2 C_F \overline{|\Delta T_{qg}^{(2)}|^2}_{C_A} \right]. \end{aligned} \quad (3.8)$$

The colour and spin average factors $K_{q\bar{q}}$ and K_{qg} are given in Eqs. (2.25) and (2.26) respectively. Further the indices C_F and C_A refer to the highest power of the colour factor multiplying the corresponding matrix elements. Finally we have also explicitly indicated the charge of the quark indicated by e_q . For the lowest order matrix elements in section 2 we have implicitly

taken it into account. However as we will see below in higher order processes the Feynman graphs contain different species of quarks. Their charges will appear in the corresponding coefficient functions and they indicate how they have to be combined with the parton densities. In NLO we encounter some new subprocesses. The first one is given by quark-quark scattering (non-identical and identical quarks) represented by

$$\begin{aligned}
q_1 + q_2 &\rightarrow q_1 + q_2 + \gamma^*, & q_1 \neq q_2, \\
\overline{|\Delta M_{q_1 q_2 \rightarrow q_1 q_2 \gamma^*}^{(2)}|^2} &= g^4 C_A C_F \left[e_{q_1}^2 \overline{|\Delta T_{q_1 q_2}^{(2)}|^2}_C + e_{q_2}^2 \overline{|\Delta T_{q_1 q_2}^{(2)}|^2}_D \right. \\
&\quad \left. + e_{q_1} e_{q_2} \overline{|\Delta T_{q_1 q_2}^{(2)}|^2}_{CD} \right], \tag{3.9}
\end{aligned}$$

$$\begin{aligned}
q + q &\rightarrow q + q + \gamma^*, \\
\overline{|\Delta M_{qq \rightarrow qq \gamma^*}^{(2)}|^2} &= g^4 C_F e_q^2 \left[C_A \left\{ \overline{|\Delta T_{q_1 q_2}^{(2)}|^2}_C + \overline{|\Delta T_{q_1 q_2}^{(2)}|^2}_D + \overline{|\Delta T_{q_1 q_2}^{(2)}|^2}_{CD} \right\} \right. \\
&\quad \left. + \overline{|\Delta T_{qq}^{(2)}|^2}_{CDEF} \right], \tag{3.10}
\end{aligned}$$

In Eqs. (3.9), (3.10) C , D , E and F refer to the graphs in Figs. 8, 9 in [30]. The second subprocess is quark-anti-quark scattering

$$\begin{aligned}
q_1 + \bar{q}_2 &\rightarrow q_1 + \bar{q}_2 + \gamma^*, & q_1 \neq q_2, \\
\overline{|\Delta M_{q_1 \bar{q}_2 \rightarrow q_1 \bar{q}_2 \gamma^*}^{(2)}|^2} &= g^4 C_A C_F \left[e_{q_1}^2 \overline{|\Delta T_{q_1 q_2}^{(2)}|^2}_C + e_{q_2}^2 \overline{|\Delta T_{q_1 q_2}^{(2)}|^2}_D \right. \\
&\quad \left. - e_{q_1} e_{q_2} \overline{|\Delta T_{q_1 q_2}^{(2)}|^2}_{CD} \right], \tag{3.11}
\end{aligned}$$

$$\begin{aligned}
q + \bar{q} &\rightarrow q_i + \bar{q}_i + \gamma^*, & q_i \neq q, \\
\overline{|\Delta M_{q\bar{q} \rightarrow q_i \bar{q}_i \gamma^*}^{(2)}|^2} &= g^4 C_A C_F \left[e_q^2 (n_f - 1) \overline{|\Delta T_{q\bar{q}}^{(2)}|^2}_A + \sum_{i=1}^{n_f-1} e_{q_i}^2 \overline{|\Delta T_{q\bar{q}}^{(2)}|^2}_B \right], \tag{3.12}
\end{aligned}$$

$$q + \bar{q} \rightarrow q + \bar{q} + \gamma^*,$$

$$\begin{aligned} \overline{|\Delta M_{q\bar{q} \rightarrow q\bar{q} \gamma^*}^{(2)}|^2} &= g^4 C_F e_q^2 \left[C_A \left\{ \overline{|\Delta T_{q\bar{q}}^{(2)}|^2}_A + \overline{|\Delta T_{q\bar{q}}^{(2)}|^2}_B + \overline{|\Delta T_{q_1 q_2}^{(2)}|^2}_C \right. \right. \\ &\quad \left. \left. + \overline{|\Delta T_{q_1 q_2}^{(2)}|^2}_D - \overline{|\Delta T_{q\bar{q}}^{(2)}|^2}_{CD} \right\} + \overline{|\Delta T_{q\bar{q}}^{(2)}|^2}_{ABCD} \right], \quad (3.13) \end{aligned}$$

and the colour average factors read

$$K_{q_1 q_2} = K_{q\bar{q}} = K_{q_1 \bar{q}_2} = K_{q\bar{q}} = \frac{1}{N^2}. \quad (3.14)$$

In Eqs. (3.11), (3.12) and (3.13) A , B , C and D refer to the graphs in Figs. 7, 8 in [30]. The last new process which shows up in NLO is given by

$$g + g \rightarrow q_i + \bar{q}_i + \gamma^*,$$

$$\overline{|\Delta M_{gg \rightarrow q_i \bar{q}_i \gamma^*}^{(2)}|^2} = g^4 \sum_{i=1}^{n_f} e_{q_i}^2 \left[C_A C_F^2 \overline{|\Delta T_{gg}^{(2)}|^2}_{C_F} + C_A^2 C_F \overline{|\Delta T_{gg}^{(2)}|^2}_{C_A} \right],$$

$$\text{with} \quad K_{gg} = \frac{1}{(N^2 - 1)^2}, \quad (3.15)$$

with the same notation as explained below Eq. (3.8). If the matrix elements are computed in n dimensions one has to be careful with the interference terms indicated by the indices CD , $CDEF$ in Eq. (3.10) and $ABCD$ in Eq. (3.13). These terms do not lead to collinear divergences so they can be computed in four dimensions. However if they are computed in n dimensions the prescription for the γ_5 -matrix leads to additional terms which are proportional $\varepsilon = n - 4$. After integration over the angles in Eq. (3.6) these terms contribute because they are multiplied by pole terms $1/\varepsilon$. Since a finite quantity cannot depend on the regularization these terms are considered to be spurious and they should be discarded. Note that without the γ_5 -matrix the terms proportional to ε cancel automatically among themselves. Some of the expressions i.e. Eqs. (3.9), (3.10), (3.12), (3.13) are singular in the limit $s_4 \rightarrow 0$, where s_4 is defined in Eq. (3.5), which is due to soft gluon radiation or soft (collinear) fermion pair production. This will lead to infrared singularities when the differential cross section in Eq. (3.5) is convoluted

with the parton densities. Therefore the cross section will be split up into a hard gluon ($s_4 > \Delta$) part and a soft gluon ($s_4 \leq \Delta$) part (see e.g. [26]). The latter is defined by

$$\begin{aligned}
s \frac{d^2 \hat{W}_{a_1 a_2}^{\text{SOFT}}}{d t d u} &= \frac{1}{2\pi} K_{a_1 a_2} \frac{S_\varepsilon^2}{(4\pi)^4 \Gamma(1 + \varepsilon)} \left(\frac{t u}{\mu^2 s} \right)^{\varepsilon/2} \\
&\times \delta(s + t + u - Q^2) \int_0^\Delta ds_4 \left(\frac{s_4}{\mu^2} \right)^{\varepsilon/2} \overline{| \Delta M_{a_1 a_2 \rightarrow b_1 b_2 \gamma^*}^{(2)} |^2}.
\end{aligned} \tag{3.16}$$

Only the singular part of $\overline{| \Delta M_{a_1 a_2 \rightarrow b_1 b_2 \gamma^*}^{(2)} |^2}$, which behaves as $1/s_4$, contributes to the above integral whereas the non-singular terms vanish in the limit $s_4 \rightarrow 0$. The calculation of the soft gluon cross section has to proceed in the same way as done for the virtual corrections in Eqs. (3.3), (3.4). First we apply the eikonal approximation to the singular part of the matrix elements and apply tensorial reduction to the soft gluon phase space integrals before we contract the Levi-Civita tensors in four dimensions. The results which hold in the HVBM- as well as RSN-schemes are given by

$$\begin{aligned}
s \frac{d^2 \Delta \hat{W}_{q\bar{q}}^{\text{SOFT}}}{d t d u} &= \delta(s + t + u - Q^2) S_\varepsilon^2 a_s^2 \frac{1}{N} \\
&\times \left[n_f C_F \left\{ -\frac{4}{3\varepsilon} - \frac{2}{3} \ln \frac{\Delta}{\mu^2} - \frac{2}{3} \ln \frac{tu}{\mu^2 s} + \frac{10}{9} \right\} \right. \\
&+ C_A C_F \left\{ -\frac{8}{\varepsilon^2} - \left(8 \ln \frac{tu}{\mu^2 s} - \frac{22}{3} \right) \frac{1}{\varepsilon} - 4 \ln \frac{\Delta}{\mu^2} \ln \frac{tu}{\mu^2 s} \right. \\
&+ 2 \ln^2 \frac{\Delta}{\mu^2} - 2 \ln^2 \frac{tu}{\mu^2 s} + \frac{11}{3} \ln \frac{\Delta}{\mu^2} + \frac{11}{3} \ln \frac{tu}{\mu^2 s} \\
&\left. \left. + 6 \zeta(2) - \frac{67}{9} \right\} \right. \\
&\left. + C_F^2 \left\{ -\frac{16}{\varepsilon^2} - \left(16 \ln \frac{\Delta}{\mu^2} \right) \frac{1}{\varepsilon} - 8 \ln^2 \frac{\Delta}{\mu^2} + 4 \zeta(2) \right\} \right]
\end{aligned}$$

$$\times |\Delta T_{q\bar{q}}^{(1)}|^2. \quad (3.17)$$

We have added the soft gluon contributions from Eqs. (3.9), (3.12) and (3.13) into the above expression. Like in the case of the virtual contribution in Eq. (3.3) the expression above is, apart from an overall minus sign and the ε -dependence of $|\Delta T_{q\bar{q}}^{(1)}|^2$, equal to the unpolarized structure function. Note that this ε -dependence leads to the breakdown of the relation in Eq. (2.62). From the reaction in Eq. (3.9) we obtain

$$\begin{aligned} s \frac{d^2 \Delta \hat{W}_{qg}^{\text{SOFT}}}{d t d u} &= \delta(s+t+u-Q^2) S_\varepsilon^2 a_s^2 \frac{1}{N} \\ &\times \left[C_A \left\{ \frac{4}{\varepsilon^2} + \left(4 \ln \frac{\Delta}{\mu^2} \right) \frac{1}{\varepsilon} + 2 \ln^2 \frac{\Delta}{\mu^2} - \zeta(2) \right\} \right. \\ &+ C_F \left\{ \frac{8}{\varepsilon^2} + \left(4 \ln \frac{\Delta}{\mu^2} + 4 \ln \frac{tu}{\mu^2 s} - 3 \right) \frac{1}{\varepsilon} + 2 \ln \frac{\Delta}{\mu^2} \ln \frac{tu}{\mu^2 s} \right. \\ &+ \ln^2 \frac{\Delta}{\mu^2} + \ln^2 \frac{tu}{\mu^2 s} - \frac{3}{2} \ln \frac{\Delta}{\mu^2} - \frac{3}{2} \ln \frac{tu}{\mu^2 s} \\ &\left. \left. - 4\zeta(2) + \frac{7}{2} \right\} \right] |\Delta T_{qg}^{(1)}|^2. \quad (3.18) \end{aligned}$$

The infrared and final state collinear divergences are cancelled upon adding the virtual contributions in Eqs. (3.3) and (3.4) to the soft gluon contributions above. The ultraviolet divergences are removed by subtracting from $d^2 \Delta \hat{W}_{a_1 a_2}^{(2)}/dt du$ ($a_1, a_2 = q, g$) the counter term

$$a_s^2(\mu^2) S_\varepsilon \frac{2\beta_0}{\varepsilon} s \frac{d^2 \Delta \hat{W}_{a_1 a_2}^{(1)}}{d t d u}, \quad \text{with} \quad \beta_0 = \frac{11}{3} C_A - \frac{4}{3} T_f n_f, \quad (3.19)$$

where we have chosen the $\overline{\text{MS}}$ renormalization scheme. Here β_0 denotes the lowest order contribution to the β -function. After renormalization one still has to perform mass factorization to remove the remaining collinear divergences. This is achieved by the formula

$$s \frac{d^2 \Delta \hat{W}_{a_1 a_2}}{d t d u}(s, t, u, \varepsilon) = \sum_{b_1, b_2=q, g} \int_0^1 \frac{dx_1}{x_1} \int_0^1 \frac{dx_2}{x_2} \Delta \Gamma_{b_1 a_1}(x_1, \varepsilon) \Delta \Gamma_{b_2 a_2}(x_2, \varepsilon)$$

$$\begin{aligned}
& \times \hat{s} \frac{d^2 \Delta W_{b_1 b_2}}{d \hat{t} d \hat{u}}(\hat{s}, \hat{t}, \hat{u}) \\
& \equiv \sum_{b_1, b_2=q, g} \Delta \Gamma_{b_1 a_1} \otimes \Delta \Gamma_{b_2 a_2} \otimes \hat{s} \frac{d^2 \Delta W_{b_1 b_2}}{d \hat{t} d \hat{u}}, \quad (3.20)
\end{aligned}$$

with the following definitions

$$\hat{s} = x_1 x_2 s, \quad \hat{t} = x_1 (t - Q^2) + Q^2, \quad \hat{u} = x_2 (u - Q^2) + Q^2. \quad (3.21)$$

In Eq. (3.20) $d^2 \Delta \hat{W}_{a_1 a_2}$ represents the singular structure functions which contain the collinear divergences indicated by ε . These divergences are removed by the kernels $\Delta \Gamma_{b_i a_i}$ leaving the finite coefficient functions $d^2 \Delta W_{b_1 b_2}$. For the RSN prescription the kernels are given in Eqs. (2.67)- (2.70). In the case of the off-shell mass assignment they are represented by the operator matrix elements in Eqs. (2.45)- (2.51). Both the kernels and the coefficient functions depend on the mass factorization scale μ . Both regularization techniques lead to the same coefficient functions renormalized in $\overline{\text{MS}}$ -scheme. The coefficient functions originating from the soft-plus-virtual gluon contributions are sufficiently short that they can be published and one can find them in Appendix A. The hard gluon parts are too long to be published. They exist as FORM [24] files and they are available on request. Here we can only show those parts which behave like $1/s_4$. In the soft gluon limit where $s_4 \rightarrow 0$ they read

$$\begin{aligned}
\lim_{s_4 \rightarrow 0} s \frac{d^2 \Delta W_{q\bar{q}}^{\text{HARD}}}{d t d u} &= a_s(\mu^2) \frac{1}{N^2} \frac{1}{s_4} \left[n_f T_f C_F \frac{4}{3} + \right. \\
&+ C_A \left\{ 4 \ln \frac{s_4}{\mu^2} - 4 \ln \frac{tu}{\mu^2 s} + \frac{11}{3} \right\} \\
&+ C_F \left\{ -16 \ln \frac{s_4}{\mu^2} + 8 \ln \frac{tu}{\mu^2 s} \right\} \left. \right] |\Delta M_{q\bar{q}}^{(1)}|^2, \quad (3.22)
\end{aligned}$$

$$\lim_{s_4 \rightarrow 0} s \frac{d^2 \Delta W_{gg}^{\text{HARD}}}{d t d u} = a_s(\mu^2) \frac{1}{N} \frac{1}{s_4} \left[C_A \left\{ 4 \ln \frac{s_4}{\mu^2} - 2 \ln \frac{tu}{\mu^2 s} \right\} \right]$$

$$+C_F \left\{ 2 \ln \frac{s_4}{\mu^2} - \frac{3}{2} \right\} \left] |\Delta M_{qg}^{(1)}|^2. \quad (3.23)$$

Another important result which emerges from our calculation is that we find the same relation as in Eq. (2.62) for the non-singlet part of the coefficient function i.e.

$$s \frac{d^2 \Delta W_{q\bar{q}}^{\text{NS},(2)}}{d t d u} = -s \frac{d^2 W_{q\bar{q}}^{\text{NS},(2)}}{d t d u}, \quad (3.24)$$

which holds for the hard and soft-plus-virtual part independently (see also the comment below Eq. (A.1)). The sum of these two parts is in agreement with Eq. (60) in [14] provided one omits the interference contribution called $2\sigma_4$ which originates from the non-singlet part of the qq -channel. The relation in Eq. (3.24) follows from chiral symmetry because the quarks are massless. Therefore the finite coefficient functions should respect this relation irrespective which regularization method is used. Finally we want to comment on the scale μ . In the computation of the radiative corrections we have assumed that the renormalization scale μ_r is equal to the mass factorization scale μ . If one wants to distinguish between these scales one has to substitute

$$a_s(\mu^2) = a_s(\mu_r^2) \left(1 + a_s(\mu_r^2) \beta_0 \ln \frac{\mu_r^2}{\mu^2} \right), \quad (3.25)$$

in all finite expressions.

4 Differential distributions for the process

$$p + p \rightarrow \gamma^* + X'$$

In this section we present the differential distributions in Eqs. (2.3), (2.4) for lepton-pair production in proton-proton collisions at the RHIC and make a comparison with similar results in previous work. In practice one is not interested in the distributions which depend on T and U in Eq. (2.2) but in the differential cross section given by

$$\frac{d^3 \Delta\sigma^{\text{PP}}}{dQ^2 d p_T d y}(S, p_T^2, y, Q^2) = 4 S Q p_T \frac{d^3 \Delta\sigma^{\text{PP}}}{dQ^2 d T d U}(S, T, U, Q^2), \quad (4.1)$$

where y and p_T denote the rapidity and transverse momentum respectively. Neglecting the masses of the incoming hadrons we have the following relations

$$\begin{aligned} T &= Q^2 - \sqrt{S} \sqrt{p_T^2 + Q^2} \cosh y + \sqrt{S} \sqrt{p_T^2 + Q^2} \sinh y, \\ U &= Q^2 - \sqrt{S} \sqrt{p_T^2 + Q^2} \cosh y - \sqrt{S} \sqrt{p_T^2 + Q^2} \sinh y. \end{aligned} \quad (4.2)$$

The kinematical boundaries are

$$Q^2 - S \leq T \leq 0, \quad -S - T + Q^2 \leq U \leq \frac{S Q^2}{T - Q^2} + Q^2, \quad (4.3)$$

from which one can derive

$$\begin{aligned} 0 \leq p_T^2 \leq p_{T,\text{max}}^2, \quad -\frac{1}{2} \ln \frac{S}{Q^2} \leq y \leq \frac{1}{2} \ln \frac{S}{Q^2}, \\ \text{with } p_{T,\text{max}}^2 = \frac{(S + Q^2)^2}{4 S \cosh^2 y} - Q^2, \end{aligned} \quad (4.4)$$

or

$$\begin{aligned} -y_{\text{max}} \leq y \leq y_{\text{max}}, \quad 0 \leq p_T^2 \leq \frac{(S - Q^2)^2}{4 S} \equiv \bar{p}_{T,\text{max}}^2, \\ \text{with } y_{\text{max}} = \frac{1}{2} \ln \frac{1 + \sqrt{1 - sq}}{1 - \sqrt{1 - sq}}, \quad sq = \frac{4 S (p_T^2 + Q^2)}{(S + Q^2)^2}. \end{aligned} \quad (4.5)$$

Since the cross section in Eq. (4.1) diverges for $p_T \rightarrow 0$ we cannot perform the integral over this kinematical variable down to zero. However the full integration over the rapidity can be carried out and one obtains the transverse momentum distribution

$$\frac{d^2 \Delta\sigma^{\text{PP}}}{dQ d p_T}(S, p_T^2, Q^2) = \int_{-y_{\text{max}}}^{y_{\text{max}}} dy \frac{d^3 \Delta\sigma^{\text{PP}}}{dQ d p_T d y}(S, p_T^2, y, Q^2), \quad (4.6)$$

with y_{max} given in Eq. (4.5). Finally we define what we mean by leading order (LO) and next-to-leading order (NLO). In LO the differential cross section is determined by the leading logarithmic approximations to the coupling constant $\alpha_s(\mu_r^2)$ in Eq. (3.25) and the polarized parton densities $\Delta f_{a_i}^P(x, \mu^2)$ in Eq. (2.4). In NLO the latter two quantities are replaced by their next-to-leading logarithmic approximations.

In the subsequent part of this section we will study the dependence of the cross sections as defined in Eqs. (4.1), (4.6) on input parameters like the QCD scale Λ , the factorization scale μ and the dependence on the chosen set of polarized parton densities. Notice that we have adopted $\mu_r = \mu$ for the renormalization scale. In our computations the number of light flavours is taken to be $n_f = 4$ which holds for the running coupling, the DY coefficient functions and the polarized parton densities. Further we have chosen for our plots the polarized parton densities provided by GRSV [40] (here called GRSV01) and BB [41], which were determined in the $\overline{\text{MS}}$ renormalization scheme. Notice that these sets do not contain charm and bottom quark densities. The densities of GRSV standard scenario were constructed to fit the available data together with positivity requirements and to satisfy two SU(3) flavour group sum rules. The GRSV collaboration have also given another set of parton densities, the so-called valence set, where the sum rules hold for the SU(2) flavour group as suggested originally in [42]. It turns out that in the standard scenario the gluon density is larger than in the valence scenario so that the DY cross section will be dominated by the qg process in the former scenario provided the transverse momentum will be sufficiently large. However in the valence scenario the sea-quark density becomes important too. Therefore there will be a competition between the qg ⁴ and $q\bar{q}$ subprocesses and it will be very hard to disentangle these two

⁴Note that the notation qg represents the subprocesses qg and $\bar{q}g$. The same holds for the notation $q\bar{q}$ representing the reactions $q\bar{q}$ and $\bar{q}q$.

densities. The BB collaboration have presented two analyses of polarized deep inelastic scattering data. At small x the densities behave as x^a where the a_G for the gluon and the a_S for the sea quark are related by $a_G = a_S + c$. In the first scenario BB assume $c = 0.9$ in LO (ISET=1) and $c = 1.0$ in NLO (ISET=3). In the second scenario BB assume $c = 0.6$ in LO (ISET=2) and $c = 0.5$ in NLO (ISET=4). All sets above are presented in LO and NLO with the Λ_4 and the corresponding values for $\alpha_s(M_Z)$ in Table 1. Besides the polarized cross sections $d\Delta\sigma$ we also want to compute the double longitudinal spin asymmetry defined by

$$A_{LL} = \frac{d\Delta\sigma}{d\sigma}, \quad (4.7)$$

where $d\sigma$ denotes the unpolarized cross section which is calculated up to NLO in [12].⁵ In order to compute the latter we adopt the GRV [43] parton density set (here called GRV98) which does not contain any charm or bottom quark densities either (for more details see Table. 1). Before presenting the results we note that our computer programs were checked by reproducing Fig.4 in [14] for the LO polarized and unpolarized nonsinglet p_T -distributions. The difference between their results and ours is numerically small which might be due to a different choice of α_s . Notice that the interference term $2\sigma_4$ mentioned below Eq. (3.24) is completely negligible. Also we reproduced several results in [10] including in particular Fig.3 for the unpolarized NLO inclusive p_T distribution and Fig. 8(b) for the LO contribution to $A_{LL}(p_T)$ in Eq. (4.7).

For our plots we choose $\sqrt{S} = 200$ GeV which is a representative C.M. energy for proton-proton collisions at the RHIC. The factorization scale is set $\mu^2 = Q^2 + p_T^2$ unless mentioned otherwise. We begin with Figs. 1a, 1b which show the p_T dependence in LO and NLO of Eq. (4.6) for $Q = 6$ GeV/c with the set GRSV01 (standard scenario). Both in LO and NLO the qg subprocess is positive but the $q\bar{q}$ channel yields larger contributions than the qg channel when $p_T < 3$ GeV/c. For larger transverse momenta the qg subprocess dominates and the $q\bar{q}$ contribution drops off rapidly where it even becomes negative when $p_T > 27$ GeV/c. At $p_T \approx 6$ GeV/c the cross section due to the $q\bar{q}$ subprocess is only one quarter of the contribution of the qg channel. Hence

⁵We re-calculated the unpolarized DY cross section and found agreement with [12]. However we used our versions of the coefficient functions for the plots in this paper.

GRSV01 (LO, standard scenario)	$\Lambda_4^{\text{LO}} = 175 \text{ MeV}$	$\alpha_s^{\text{LO}}(M_Z) = 0.121$
GRSV01 (NLO, standard scenario)	$\Lambda_4^{\text{NLO}} = 257 \text{ MeV}$	$\alpha_s^{\text{NLO}}(M_Z) = 0.109$
GRSV01 (LO, valence scenario)	$\Lambda_4^{\text{LO}} = 175 \text{ MeV}$	$\alpha_s^{\text{LO}}(M_Z) = 0.121$
GRSV01 (NLO, valence scenario)	$\Lambda_4^{\text{NLO}} = 257 \text{ MeV}$	$\alpha_s^{\text{NLO}}(M_Z) = 0.109$
BB (LO, scenario 1)	$\Lambda_4^{\text{LO}} = 203 \text{ MeV}$	$\alpha_s^{\text{LO}}(M_Z) = 0.123$
BB (NLO, scenario 1)	$\Lambda_4^{\text{NLO}} = 235 \text{ MeV}$	$\alpha_s^{\text{NLO}}(M_Z) = 0.107$
BB (LO, scenario 2)	$\Lambda_4^{\text{LO}} = 195 \text{ MeV}$	$\alpha_s^{\text{NLO}}(M_Z) = 0.123$
BB (NLO, scenario 2)	$\Lambda_4^{\text{NLO}} = 240 \text{ MeV}$	$\alpha_s^{\text{NLO}}(M_Z) = 0.107$
GRV98 (LO)	$\Lambda_4^{\text{LO}} = 175 \text{ MeV}$	$\alpha_s^{\text{NLO}}(M_Z) = 0.121$
GRV98(NLO)	$\Lambda_4^{\text{NLO}} = 257 \text{ MeV}$	$\alpha_s^{\text{NLO}}(M_Z) = 0.109$

Table 1: Polarized and unpolarized parton density sets with the values for the QCD scale Λ_4 and the running coupling $\alpha_s(M_Z)$.

we see that when $p_T > Q/2$ the qg channel begins to dominate over the other subprocesses. The NLO results from all subprocesses are presented in Fig.1b where we note that the contributions from the gg and qq channels are small and negative so that we plot their absolute values. The possibility that the polarized gluon density can be measured in the DY process at large p_T has already been stressed by several authors using LO perturbation expressions, for recent work see [10]. We have now demonstrated that this conclusion is unaltered when the NLO contributions are included.

In Figs. 2a, 2b we do the same as in Figs. 1a, 1b but now the plots are presented for the GRSV01 valence scenario. In this case the $q\bar{q}$ channel also dominates the cross section at small transverse momenta but this contribution is negative over the whole p_T range so we plot its absolute value. On the other hand the qg subprocess only yields positive contributions. The net effect is that below $p_T \sim 5 \text{ GeV}/c$ the LO polarized cross section due to both contributions is negative because the $q\bar{q}$ reaction is dominant in this region. For $p_T > 5 \text{ GeV}/c$ the LO cross section becomes positive since in this region the qg -channel is more important. Hence we plot the absolute value of LO(sum) in Fig. 2a. This overall picture is not altered by including the NLO corrections so also the NLO(sum) is negative for small p_T and positive for large p_T and we add the plot of its absolute value to Fig.2a. In Fig. 2b we show the individual NLO contributions. The gg and qq channels are small

and negative so we have plotted their absolute values. Therefore the main difference between the standard and valence scenarios shows up in the region $p_T < 5$ GeV/c where the standard scenario provides us with a positive NLO distribution while the valence scenario yields a negative one. Note that there is nothing unphysical about this result because the polarized cross section is the difference between two helicity projections. If the valence scenario is correct one will need high statistics in the region where the p_T distribution changes sign, say for $4 < p_T < 6$ GeV/c.

Given the changes in signs in the above results it is clear that rapidity plots integrated over a range in p_T will depend strongly on the range available experimentally and will also vary dramatically. Therefore we will only present the rapidity distributions in Eq. (4.1), at a fixed representative p_T . In Figs. 3a, 3b we show the LO and NLO corrected distributions with $Q = 6$ GeV/c and $p_T = 2$ GeV/c using the GRSV01 standard scenario parton densities. In this region the $q\bar{q}$ channel dominates the cross section and it leads to a positive contribution in the whole rapidity range. Since the qg channel has two maxima at symmetric values of y the total LO distribution has a slight minimum at $y = 0$ which is enhanced when the NLO corrections are taken into account. This is explained by Fig. 3b where we see that the qg , gg and $q\bar{q}$ contributions are all negative near $y = 0$ so the dip is more pronounced. At larger p_T the relative contributions from these channels changes but the qg becomes a larger fraction of the total so that the double peaked nature of the NLO distribution will remain. We repeat these two plots for the valence scenario parton densities in Figs. 4a and 4b. However we have now chosen $p_T = 6$ GeV/c where the both the LO and NLO cross sections are positive. Here one clearly sees that the rapidity distributions are negative near $y = 0$, where they have pronounced minima. This is wholly due to the $q\bar{q}$ subprocess which yields negative contributions to the cross section over the whole rapidity range. The qg subprocess is positive for all values of the rapidity and compensates the $q\bar{q}$ contribution leaving a much smaller cross section than shown by the standard scenario in Figs. 3a, 3b. This was already expected from the transverse momentum distributions in Figs. 2a,2b where the cross section decreases at small values of p_T and is actually negative for $p_T < 5$ GeV/c. At larger p_T the double peaked nature of this distribution will prevail as the relative contribution from the qg channel increases. Note that the integrals over the above rapidity distributions agree with the values of the p_T distributions in Figs. 1a, 1b and Figs. 2a, 2b at

$p_T = 2$ and $p_T = 6$ GeV/c respectively.

In Fig. 5 we have shown the LO and NLO corrected cross sections for the GRSV01 standard scenario at different values for the di-lepton pair invariant mass Q . When we increase the value of Q the p_T distributions decrease in LO as well as in NLO. Further we observe that the NLO corrections become larger when the transverse momentum increases. This will become more clear when we show the K -factor later on. The dependence on Q is also investigated for the y -distributions shown in Fig. 6. Here the the NLO correction is conspicuous at $Q = 2$ GeV/c whereas at larger values of Q there are hardly any differences between the LO and NLO corrected cross sections.

Radiative corrections are marred by theoretical uncertainties. The first one concerns the choice of the factorization and renormalization scale μ . Since the perturbation series is truncated at a certain order of α_s physical quantities depend on μ . Notice that this dependence will disappear when all orders are taken into account. The sensitivity to the scale above is exhibited by the ratio

$$N\left(\frac{\mu}{\mu_0}\right) = \frac{d\Delta\sigma(\mu)}{d\Delta\sigma(\mu_0)}. \quad (4.8)$$

If this ratio is close to unity and almost independent of μ the higher order corrected cross section will be very reliable. In Fig. 7a we use the GRSV01 standard scenario and investigate the ratio in Eq. (4.8) for the cross section in Eq. (4.6). Here we choose as central value $\mu_0^2 = Q^2 + p_T^2$ and we vary μ from $0.2 \mu_0$ to $5\mu_0$ at $Q = 8$ GeV/c. Note that the scale on the μ/μ_0 -axis is logarithmic. For the transverse momenta we take $p_T = 2, 10$ and 20 GeV/c. In Fig. 7a the LO corrected $N(p_T, \mu/\mu_0)$ are the upper curves for small μ/μ_0 whereas the lower curves are the NLO corrected $N(p_T, \mu/\mu_0)$. One sees that the scale dependence diminishes in going from LO to NLO which indicates better predictive power in NLO perturbation theory. The analogous plot is shown in Fig. 7b for $d^3\Delta\sigma(p_t, y, \mu)/dQdp_Tdy$ as a function of y , with $y = 0$ and $y = \pm 1$ where now $\mu_0^2 = Q^2 + p_T^2$ and $p_T = 2$ GeV/c. Since the y -plots are symmetric the values at $y = 1$ are identical to those for $y = -1$ so there are only four curves in Fig. 7b. Again the LO curves are above the NLO ones for small μ/μ_0 . Like in the case of the transverse momentum distributions there is an improvement in the scale dependence in going from LO to NLO perturbation theory.

Besides the dependence on the factorization/renormalization scales there are two other uncertainties which affect the predictive power of the theoretical cross section. The first one concerns the rate of convergence of the perturbation series which is indicated by the K -factor defined by

$$K = \frac{d\Delta\sigma^{\text{NLO}}}{d\Delta\sigma^{\text{LO}}}. \quad (4.9)$$

This quantity is plotted as a function of p_T in Fig. 8a for $Q = 2, 6$ and 10 GeV/c in the GRSV standard scenario and we see that it varies from approximately 1.2 at $p_T = 2$ GeV/c to 1.7 at $p_T = 30$ GeV/c. The corresponding rapidity plots for fixed $p_T = 2$ GeV/c in Fig. 8b vary from 0.8 to 1.5 for the case of $Q = 2$ GeV/c and from 1.2 to 1.5 for the case of $Q = 6$ GeV/c. Notice the dips around $y = 0$. They are explained in the discussion of Figs. 3a,3b. The minimum in the LO rapidity distribution becomes deeper when the NLO corrections, mainly coming from the qg subprocess, are included. The study of the K -factors reveal that the NLO corrections are appreciable (sometimes more than 50%) except at small p_T where fortunately the cross section attains its maximum.

A third uncertainty which has to be solved by experiment are the parton densities originating from different parametrizations. To study the dependence on these densities it is better to reduce the effect of the choice of factorization scale and the various K -factors. This is achieved by plotting the double longitudinal spin asymmetry as given by Eq. (4.7). Besides the GRSV01 parton density sets we also include the sets presented in [41].

We show the LO double longitudinal spin asymmetry versus p_T in Fig. 9a and the corresponding NLO result in Fig. 9b for $Q = 6$ GeV/c and $\sqrt{S} = 200$ GeV. They are integrated over y and the results are given in percent. The BB set 1 shows the most dramatic rise in A_{LL} when p_T increases, while the other scenarios only show moderate increases. This is because the polarized gluon density in this set is larger than those contained in the other sets. Note that in the GRSV01 valence scenario A_{LL} is negative in LO and NLO below $p_T \sim 5$ GeV/c which can be inferred from Figs. 2a and 2b. However if the value of $A_{LL}(p_T)$ is as small as indicated here this effect will not be measurable. A more direct comparison of the NLO results for $A_{LL}(p_T)$ in Fig. 9b with the LO results in Fig. 9a is provided by the ratios of the two plots which is given in Fig.9c. The strange behaviour of the GRSV01 valence scenario below $p_T = 6$ GeV/c is due to the change in signs in the

LO and NLO results. We see that this ratio is close to unity for the GRSV standard scenario and the BB, set 1 while it is smaller for the BB, set 2. This reflects the fact that the K -factors in the polarized and unpolarized p_T distributions are almost equal. In Figs. 10a and 10b we show the LO and NLO results for $A_{LL}(p_T, y)$ as a function of y at $Q = 6$ GeV/c and $p_T = 6$ GeV/c. For these values the qg contribution dominates and the cross section is positive. Since the cross sections for the GRSV01 valence scenario in Figs. 4a,4b are small at this p_T and fluctuate in sign across the rapidity range it is likely that $A_{LL}(p_T, y)$ will not be large as a function of y so we have omitted this parametrization in Figs. 10a-c. Again we see that the BB set 1 distributions yield the largest results. We also take the ratios of the plots in Figs. 10b divided by those in Figs. 10a, which are presented in Fig. 10c. The latter reveals that the ratio between the LO and NLO corrected longitudinal asymmetry deviates considerably from unity for the BB sets in particular for set 2. This means that the K -factors for these sets differ from those computed for the unpolarized cross sections. In the central rapidity region the results are below unity reflecting the negative NLO contributions found earlier. From Figs. 9b, 10b we can conclude that one can only distinguish between the various parton densities when the polarized gluon density is very large. In the case of the GRSV-set one cannot measure the difference between the valence and the standard scenario. Even the difference between the GRSV scenarios and scenario 2 of the BB-set is very small. If we assume that the proton beams have 100 % polarization (75% is more likely) we need to know the polarized cross sections up to 7% to obtain A_{LL} in Fig. 9b at $p_T = 20$ GeV/c up to 12.5%. This is necessary to distinguish between the GRSV set and BB, set 2 which is very unlikely. However if the error on the polarized cross sections is 17% then A_{LL} at $p_T = 20$ GeV/c can be determined up to 25% which is sufficient to distinguish between scenarios 1 and 2 of the BB-set.

Summarizing the above we have calculated the NLO corrections to the single particle inclusive distributions for lepton-pair production in polarized proton-proton scattering. We used the approximation that the lepton pair emerges from a virtual photon only and we neglected the additional contributions coming from the Z -boson production which is quite valid as long as $Q < 50$ GeV/c. A part of the calculation was performed using two different regularization methods to deal with the spurious terms introduced by the prescription for the γ_5 -matrix if the matrix elements are computed in

n dimensions. The coefficient functions are presented in the standard $\overline{\text{MS}}$ scheme. In this scheme the non-singlet polarized and unpolarized coefficient functions satisfy the relation $\Delta W_{q\bar{q}} = -W_{q\bar{q}}$ which are strong checks on our calculations. We have presented some NLO results for quantities of experimental interest. The fact that the qg channel yields the largest contribution at moderate p_T indicates that experimental measurements of the DY p_T distribution will give us information on the polarized gluon density provided the latter is sufficiently large. We found that the K factors are moderate at least in the small p_T -range and that there is a reduction in the scale dependence of the inclusive distributions in NLO as compared with LO. It is now up to the experimental groups working on polarized proton-proton scattering at RHIC to measure these DY distributions.

Acknowledgement: We thank M. Klasen for discussions regarding the plots in [10] and C. Coriano for a clarification of the results in [14].

Appendix A

Here we list the soft-plus-virtual gluon contributions to the polarized DY coefficient functions which are determined by the one-loop corrections to the processes in Eqs. (2.25), (2.26) and the soft gluon corrections due to reactions (3.7), (3.9). The $q\bar{q}$ reaction yields the result

$$\begin{aligned}
s \frac{d^2 \Delta \hat{W}_{q\bar{q}}^{S+V}}{d t d u} &= \delta(s+t+u-Q^2) S_\varepsilon^2 a_s^2 \frac{1}{N} \\
&\times \left[n_f C_F \left\{ -\frac{2}{3} \ln \frac{\Delta}{\mu^2} + \frac{10}{9} \right\} |\Delta T_{q\bar{q}}^{(1)}|^2 \right. \\
&+ C_F(C_F - C_A/2) \left\{ -4 \ln^2 \frac{\Delta}{\mu^2} + 4 \ln \frac{tu}{\mu^2 s} \ln \frac{\Delta}{\mu^2} \right. \\
&- 4 \text{Li}_2 \left(\frac{s-Q^2}{s} \right) - 4 \text{Li}_2 \left(\frac{t}{Q^2} \right) - 4 \ln^2 \frac{-t}{\mu^2} - 2 \ln^2 \frac{s}{\mu^2} \\
&- 2 \ln \frac{-t}{\mu^2} \ln \frac{-u}{\mu^2} + 8 \ln \frac{-t}{\mu^2} \ln \frac{s}{\mu^2} + 2 \ln^2 \left(\frac{t-Q^2}{t} \right) \\
&\left. \left. - 2 \ln^2 \left(\frac{Q^2-t}{Q^2} \right) - 3 \ln \frac{Q^2}{\mu^2} - 6 \zeta(2) + 8 + (t \Leftrightarrow u) \right\} \right. \\
&\times |\Delta T_{q\bar{q}}^{(1)}|^2 \\
&+ C_A C_F \left\{ -\ln^2 \frac{\Delta}{\mu^2} + \frac{11}{6} \ln \frac{\Delta}{\mu^2} - 2 \text{Li}_2 \left(\frac{t}{Q^2} \right) \right. \\
&+ \ln \frac{-t}{\mu^2} \ln \frac{-u}{\mu^2} + \ln^2 \left(\frac{t-Q^2}{t} \right) - \ln^2 \left(\frac{Q^2-t}{Q^2} \right) - \frac{3}{2} \ln \frac{Q^2}{\mu^2} \\
&\left. \left. - 3 \zeta(2) + \frac{5}{18} + (t \Leftrightarrow u) \right\} |\Delta T_{q\bar{q}}^{(1)}|^2
\end{aligned}$$

$$\begin{aligned}
& +C_F(C_F - C_A/2) \left\{ \frac{16s + 8t}{u} \left(\text{Li}_2 \left(\frac{t}{Q^2} \right) + \text{Li}_2 \left(\frac{s - Q^2}{s} \right) \right. \right. \\
& + \frac{1}{2} \ln^2 \frac{-t}{s} - \frac{1}{2} \ln^2 \left(\frac{t - Q^2}{t} \right) + \frac{1}{2} \ln^2 \left(\frac{Q^2 - t}{Q^2} \right) \left. \right) \\
& + \frac{8s(s - 2Q^2)}{(s - Q^2)^2} \ln \frac{s}{Q^2} + \left(\frac{4tu}{(Q^2 - t)^2} - \frac{8(t - 2u)}{Q^2 - t} - 16 \right) \\
& \times \ln \frac{-t}{Q^2} + \frac{4(s + u)}{t} + \frac{8s}{s - Q^2} + \frac{4u}{Q^2 - t} - 4 + (t \Leftrightarrow u) \left. \right\} \\
& + C_A C_F \left\{ \left(\frac{2tu}{(Q^2 - t)^2} + \frac{8(u - t)}{Q^2 - t} - 8 \right) \ln \frac{-t}{Q^2} - \frac{2(s + u)}{t} \right. \\
& \left. + \frac{2u}{Q^2 - t} - 2 + (t \Leftrightarrow u) \right\}, \tag{A.1}
\end{aligned}$$

which, apart from an overall minus sign, is equal to the unpolarized soft-plus-virtual gluon contributions to the unpolarized DY coefficient function. The qg subprocess provides us with the result

$$\begin{aligned}
s \frac{d^2 \Delta \hat{W}_{qg}^{\text{S+V}}}{d t d u} &= \delta(s + t + u - Q^2) S_\varepsilon^2 a_s^2 \frac{1}{N} \\
& \times \left[C_F \left\{ \ln^2 \frac{\Delta}{\mu^2} - \frac{3}{2} \ln \frac{\Delta}{\mu^2} + 2 \text{Li}_2 \left(\frac{t}{Q^2} \right) + 2 \text{Li}_2 \left(\frac{u}{Q^2} \right) \right. \right. \\
& - 2 \ln \frac{-t}{\mu^2} \ln \frac{-u}{\mu^2} + \ln^2 \frac{-t}{\mu^2} - \ln^2 \left(\frac{t - Q^2}{t} \right) \\
& - \ln^2 \left(\frac{u - Q^2}{u} \right) + \ln^2 \left(\frac{Q^2 - t}{Q^2} \right) + \ln^2 \left(\frac{Q^2 - u}{Q^2} \right) \\
& \left. + 3 \ln \frac{Q^2}{\mu^2} + 8 \zeta(2) - \frac{11}{2} \right\} |\Delta T_{qg}^{(1)}|^2
\end{aligned}$$

$$\begin{aligned}
& +C_A \left\{ 2 \ln^2 \frac{\Delta}{\mu^2} - 2 \ln \frac{tu}{\mu^2 s} \ln \frac{\Delta}{\mu^2} + \text{Li}_2 \left(\frac{s-Q^2}{s} \right) \right. \\
& - \text{Li}_2 \left(\frac{u}{Q^2} \right) + 2 \ln \frac{-t}{\mu^2} \ln \frac{-u}{s} + \frac{1}{2} \ln^2 \frac{u}{s} + \frac{1}{2} \ln^2 \left(\frac{u-Q^2}{u} \right) \\
& \left. - \frac{1}{2} \ln^2 \left(\frac{Q^2-u}{Q^2} \right) - 2\zeta(2) + 1 \right\} |\Delta T_{gg}^{(1)}|^2 \\
& +C_F \left\{ \frac{4(t+2u)}{s} \left(-\text{Li}_2 \left(\frac{s-Q^2}{s} \right) + \text{Li}_2 \left(\frac{t}{Q^2} \right) \right. \right. \\
& - \ln \frac{-u}{\mu^2} \ln \frac{-t}{s} + \frac{1}{2} \ln^2 \frac{-t}{\mu^2} - \frac{1}{2} \ln^2 \frac{s}{\mu^2} - \frac{1}{2} \ln^2 \left(\frac{t-Q^2}{t} \right) \\
& \left. + \frac{1}{2} \ln^2 \left(\frac{Q^2-t}{Q^2} \right) + 5\zeta(2) \right) + \left(\frac{2su}{(s-Q^2)^2} - \frac{2(s+4u)}{s-Q^2} \right) \\
& \times \ln \frac{s}{Q^2} + \left(\frac{2st}{(Q^2-t)^2} + \frac{4(2s-t)}{Q^2-t} - 8 \right) \ln \frac{-t}{Q^2} - \frac{2u}{s} + \frac{2u}{t} \\
& \left. + \frac{2s}{Q^2-t} - \frac{2u}{s-Q^2} - 2 \right\} \\
& +C_A \left\{ \frac{2(t+2u)}{s} \left(\text{Li}_2 \left(\frac{s-Q^2}{s} \right) - \text{Li}_2 \left(\frac{t}{Q^2} \right) \right. \right. \\
& + \ln \frac{-u}{\mu^2} \ln \frac{-t}{s} - \frac{1}{2} \ln^2 \frac{-t}{\mu^2} + \frac{1}{2} \ln^2 \frac{s}{\mu^2} + \frac{1}{2} \ln^2 \left(\frac{t-Q^2}{t} \right) \\
& \left. - \frac{1}{2} \ln^2 \left(\frac{Q^2-t}{Q^2} \right) - 5\zeta(2) \right) - \frac{2s}{s-Q^2} \ln \frac{s}{Q^2} \\
& \left. - \frac{2t}{Q^2-t} \ln \frac{-t}{Q^2} + \frac{2u}{s} - \frac{2u}{t} \right\} \Bigg]. \tag{A.2}
\end{aligned}$$

References

- [1] G. Bunce, N. Saito, J. Soffer and W. Vogelsang, *Ann. Rev. Nucl. Part. Sci.* **50** (2000) 525.
- [2] I. Bojak and M. Stratmann, *Phys. Lett.* **B433** (1998) 411, *ibid.* *Nucl.Phys.* **B540** (1999) 345;
Z. Merebashvili, A.P. Contogouris and G. Grispos, *Phys. Rev.* **D62** (2000) 114509.
- [3] A.P. Contogouris, B. Kamal, Z. Merebashvili and F.V. Tkachov, *Phys. Lett.* **B304** 329, *ibid* *Phys. Rev.* **D48** (1993) 4092.
- [4] L.E. Gordon and W. Vogelsang, *Phys. Rev.* **D48** (1993) 3136, **D49** (1994) 170.
- [5] I. Bojak and M. Stratmann, hep-ph/0112276.
- [6] A. Weber, *Nucl. Phys.* **B382** (1992) 63.
- [7] T. Gehrmann, *Nucl. Phys.* **B498** (1997) 245, **B534** (1998) 21.
- [8] B. Kamal, *Phys. Rev.* **D53** (1996) 1142, **D57** (1998) 6663.
- [9] E.L. Berger, L.E. Gordon and M. Klasen, *Phys. Rev.* **D58** (1998) 074012.
- [10] E.L. Berger, L.E. Gordon and M. Klasen, *Phys. Rev.* **D62** (2000) 014014.
- [11] R.K. Ellis, G. Martinelli and R. Petronzio, *Nucl. Phys.* **B211** (1983) 106.
- [12] B. Arnold and M.H. Reno, *Nucl. Phys.* **B319** (1989) 37, Erratum *ibid.* **B330** (1990) 284;
R. J. Gonsalves, J. Pawlowski and C-F. Wai, *Phys. Rev.* **D40** (1989) 2245.
- [13] S. Chang, C. Coriano, R.D. Field and L.E. Gordon, *Phys. Lett.* **B403** (1997) 344, *ibid.* *Nucl. Phys.* **B512** (1998) 393.

- [14] S. Chang, C. Coriano and R.D. Field, Nucl. Phys. **B528** (1998) 285.
B528 (1998) 285.
- [15] C.G. Bollini and J.J. Giambiagi, Nucl. Phys. **B97** (1975) 522, *ibid.* "Rio De Janiero 1974, Fifth Brazilian Symposium On Theoretical Physics, Vol. 1", Rio De Janiero 1975, 335;
M. Bos, Ann. Phys. (NY) **181** (1988) 177;
C. Schubert, Nucl. Phys. **B323** (1989) 478;
C.P. Martin and D. Sanchez-Ruiz, Nucl. Phys. **B572** (2000) 387.
- [16] G. 't Hooft and M. Veltman, Nucl. Phys. **B44** (1972) 189.
- [17] P. Breitenlohner and B. Maison, Commun. Math. **53** (1977) 11, 39, 55.
- [18] S.A. Larin, Phys. Lett. **B303** (1993) 113, **B334** (1994) 192.
- [19] R. Mertig and W.L. van Neerven, Z. Phys. **C70** (1996) 637.
- [20] W. Vogelsang, Phys. Rev. **D54** (1996) 2023, Nucl. Phys. **B475** (1996) 47.
- [21] Y. Matiounine, J. Smith and W.L. van Neerven, Phys. Rev. **D58** (1998) 076002.
- [22] W.L. van Neerven, Acta Phys. Polon. **B29** (1998) 1175.
- [23] B. Humpert and W.L. van Neerven, Phys. Lett. **B84** (1979) 327, Erratum-*ibid* **B85** (1979) 471, **B89** (1979) 69, Nucl. Phys. **B178** (1981) 498, *ibid* **B184** (1981) 225.
- [24] FORM by J.A.M. Vermaseren, version 3.0 available from <http://www.nikhef.nl/form>.
- [25] D. Akyeampong and R. Delbourgo, Nuov. Cim. **17A** (1973) 578, **18A** (1973) 94, **19A** (1974) 219.
- [26] V. Ravindran, J. Smith and W.L. van Neerven, Nucl. Phys. **B634** (2002) 247..
- [27] S.L. Adler, Phys. Rev. **177** (1969) 2426;
J.S Bell and R. Jackiw, Nuovo Cim. **A60** (1969) 47.

- [28] S.L. Adler and W. Bardeen, Phys. Rev. **182** (1969) 1517.
- [29] W. Pauli and F. Villars, Rev. Mod. Phys. **21** (1949) 434.
- [30] T. Matsuura, R. Hamberg and W.L. van Neerven, Nucl. Phys. **B359** (1991) 343.
- [31] A.N. Schellekens and W.L. van Neerven, Phys. Rev. **D21** (1980) 2619; **D22** (1980) 1623.
- [32] B. Humpert and W.L. van Neerven, Phys. Lett. **B101** (1981) 101, Phys. Rev. **D24** (1981) 2245.
- [33] T. Kinoshita, J. Math. Phys. **3** (1962) 650.
- [34] G. Passarino and M. Veltman, Nucl. Phys. **B160** (1979) 151.
- [35] W. Beenakker, PhD. thesis, Universiteit Leiden, 1989.
- [36] P. Mathews and V. Ravindran, Mod. Phys. Lett. **A7** (1992) 2695.
- [37] W. Beenakker, H. Kuijf, W.L. van Neerven and J. Smith, Phys. Rev. **D40** (1989) 54.
- [38] T. Matsuura, S.C. van der Marck and W.L. van Neerven, Nucl. Phys. **B319** (1989) 570.
- [39] L. Lewin, "Polylogarithms and Associated Functions", North Holland, Amsterdam, 1983.
- [40] M. Glück, E. Reya, M. Stratmann and W. Vogelsang, Phys. Rev. **D63** (2001) 094005.
- [41] J. Blumlein and H. Böttcher, DESY-01-087, hep-ph/0203155.
- [42] H.J. Lipkin, Phys. Lett. **B256** (1991) 284; **B337** (1994) 157; J. Lichtenstadt and H.J. Lipkin, Phys. Lett. **B353** (1995) 119.
- [43] M. Glück, E. Reya and A. Vogt, Eur. Phys. J. **C5** (1998) 461.

Figure Captions

- Fig. 1a.** The LO differential cross section $d^2\Delta\sigma/dQ dp_T$ at $\sqrt{s} = 200$ GeV for the GRSV01 standard scenario plotted in the range $2 < p_T < 30$ GeV/c with $Q = 6$ GeV/c² and $\mu^2 = Q^2 + p_T^2$. The LO plots are for the subprocesses $q\bar{q}$ (dot-dashed line), qg (dashed line) and the sum (dotted line). For convenience we also add the NLO result (solid line) from Fig. 1b.
- Fig. 1b.** Same as Fig. 1a but now for NLO. Further we have shown the contributions from all subprocesses $q\bar{q}$ (dot-dashed line), qg (long-dashed line), gg (dotted line) and qq (short-dashed line). The latter two reactions yield negative contributions we plot their absolute values.
- Fig. 2a.** Same as in Fig. 1a but now using GRSV01 valence scenario. Since the $q\bar{q}$ contribution is negative at small p_T we plot its absolute value. For convenience we also add the NLO result (solid line) from Fig. 2b.
- Fig. 2b.** Same as in Fig. 1b but now using GRSV01 valence scenario. Again we plot absolute values when the contributions are negative.
- Fig. 3a.** The LO differential cross section $d^3\Delta\sigma/dQ dp_T dy$ at $\sqrt{s} = 200$ GeV for the GRSV01 standard scenario with $Q = 6$ GeV/c², $p_T = 2$ GeV/c and $\mu^2 = Q^2 + p_T^2$. The LO plots are for the subprocesses $q\bar{q}$ (dot-dashed line), qg (dashed line) and the sum (dotted line). For convenience we also add the NLO result (solid line) from Fig. 3b.
- Fig. 3b.** Same as Fig. 3a but now for NLO. Further we have shown the contributions from all subprocesses $q\bar{q}$ (dot-dashed line), qg (long-dashed line), gg (dotted line) and qq (short-dashed line).
- Fig. 4a.** Same as in Fig. 3a but now using GRSV01 valence scenario and at $p_T = 6$ GeV/c.
- Fig. 4b.** Same as in Fig. 3b but now using GRSV01 valence scenario and at $p_T = 6$ GeV/c.
- Fig. 5.** The dependence of $d^2\Delta\sigma/dQ dp_T$ on p_T at $\sqrt{s} = 200$ GeV with the GRSV01 standard scenario and $\mu^2 = Q^2 + p_T^2$. Reading from top to

bottom the solid lines are the NLO results for $Q = 2, 6,$ and $10 \text{ GeV}/c^2$ and the dashed lines are the LO results.

Fig. 6. The dependence of $d^3\Delta\sigma/dQ dp_T dy$ on y at $\sqrt{s} = 200 \text{ GeV}$ and $p_T = 2 \text{ GeV}/c$ with the GRSV01 standard scenario and $\mu^2 = Q^2 + p_T^2$. Reading from top to bottom the solid lines are the NLO results for $Q = 2, 6,$ and $10 \text{ GeV}/c^2$ and the dashed lines are the LO results.

Fig. 7a. The quantity $N(p_T, \mu/\mu_0)$ (Eq. (4.8)) plotted in the range $0.2 < \mu/\mu_0 < 5$ (logarithmic scale) with $Q = 8 \text{ GeV}/c^2$ and $\mu_0^2 = Q^2 + p_T^2$. The results are shown for $p_T = 2 \text{ GeV}/c$ (solid line), $p_T = 10 \text{ GeV}/c$ (dashed line), $p_T = 20 \text{ GeV}/c$ (dot-dashed line). The three upper curves on the left hand side are the LO results whereas the three lower curves are the NLO results.

Fig. 7b. The quantity $N(p_T, y, \mu/\mu_0)$ (analogous to Eq. (4.8)) plotted at $p_T = 2 \text{ GeV}/c$ in the range $0.2 < \mu/\mu_0 < 5$ (logarithmic scale) with $Q = 8 \text{ GeV}/c^2$ and $\mu_0^2 = Q^2 + p_T^2$. The results are shown for $y = \pm 1$ (solid line) and $y = 0$ (dashed line). The two upper curves on the left hand side are the LO results whereas the two lower curves are the NLO results.

Fig. 8a. The K -factor (Eq. (4.9)) for $d^2\Delta\sigma/dQ dp_T$ plotted in the range $2 < p_T < 30 \text{ GeV}/c$ for $\mu^2 = Q^2 + p_T^2$. The values for Q are $Q = 2 \text{ GeV}/c^2$ (solid line), $Q = 6 \text{ GeV}/c^2$ (dashed line) and $Q = 10 \text{ GeV}/c^2$ (dot-dashed line).

Fig. 8b. The K -factor (Eq. (4.9)) for $d^3\Delta\sigma/dQ dp_T dy$ at $p_T = 2 \text{ GeV}/c$ with $\mu^2 = Q^2 + p_T^2$. The values for Q are $Q = 2 \text{ GeV}/c^2$ (solid line), $Q = 6 \text{ GeV}/c^2$ (dashed line) and $Q = 10 \text{ GeV}/c^2$ (dot-dashed line).

Fig. 9a. The LO longitudinal asymmetry $A_{LL}(p_T)$ (Eq. (4.7)) in % plotted in the range $2 < p_T < 30 \text{ GeV}/c$ for $Q = 6 \text{ GeV}/c^2$ and $\mu^2 = Q^2 + p_T^2$. GRSV01, standard scenario (solid line), GRSV01, valence scenario (dashed line), BB, set 1 (dot-dashed line) and BB, set 2 (dotted line).

Fig. 9b. Same as in Fig. 9a but now for $A_{LL}(p_T)$ (Eq. (4.7)) in NLO.

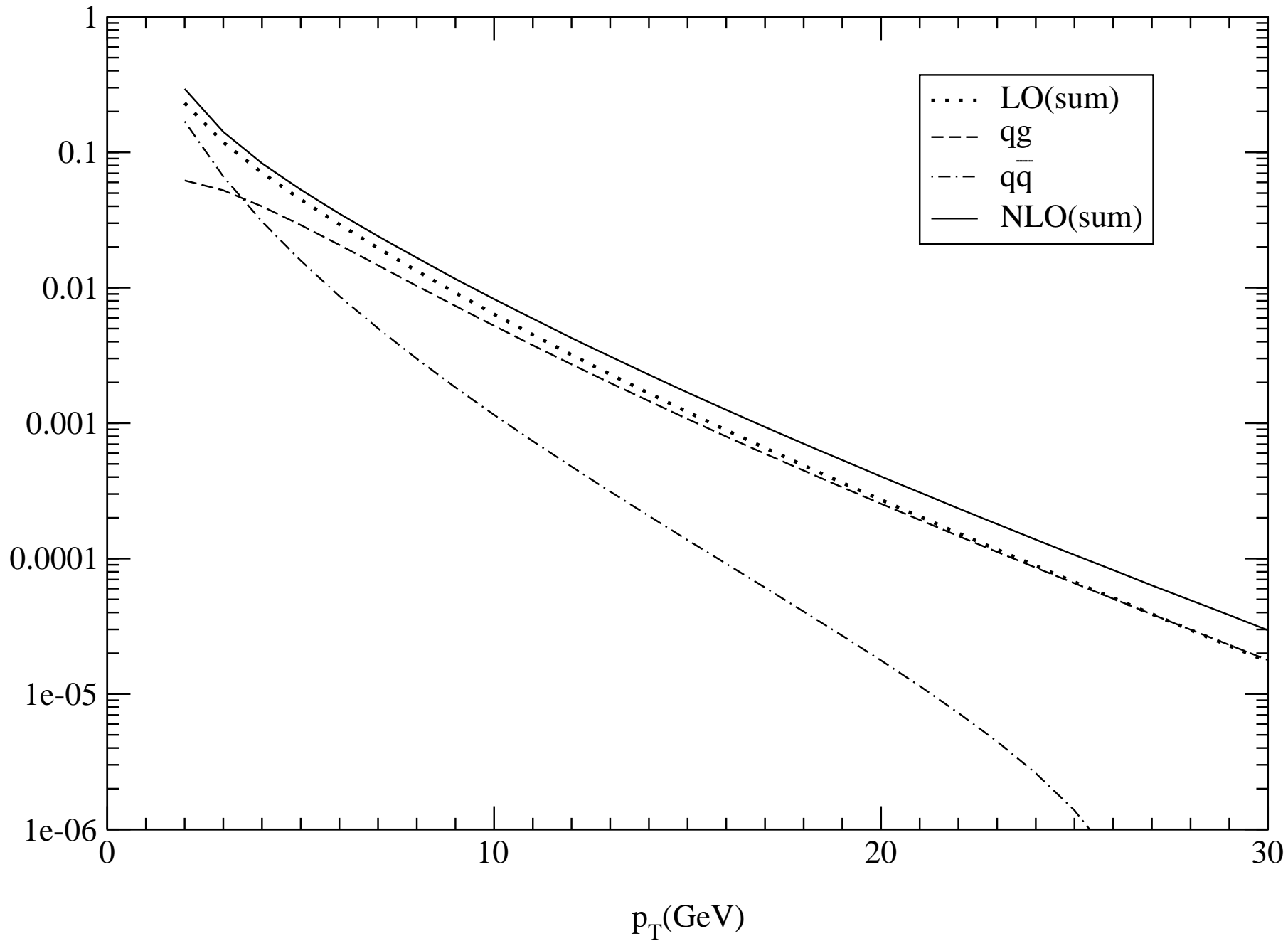
Fig. 9c. The ratio of $A_{LL}(p_T)$ in NLO in Fig. 9b divided by $A_{LL}(p_T)$ in LO in Fig. 9a.

Fig. 10a. The LO longitudinal asymmetry $A_{LL}(p_T, y)$ (Eq. (4.7)) in % at $p_T = 6 \text{ GeV}/c$ for $Q = 6 \text{ GeV}/c^2$ and $\mu^2 = Q^2 + p_T^2$. GRSV01, standard scenario (solid line), BB, set 1 (dot-dashed line) and BB, set 2 (dotted line).

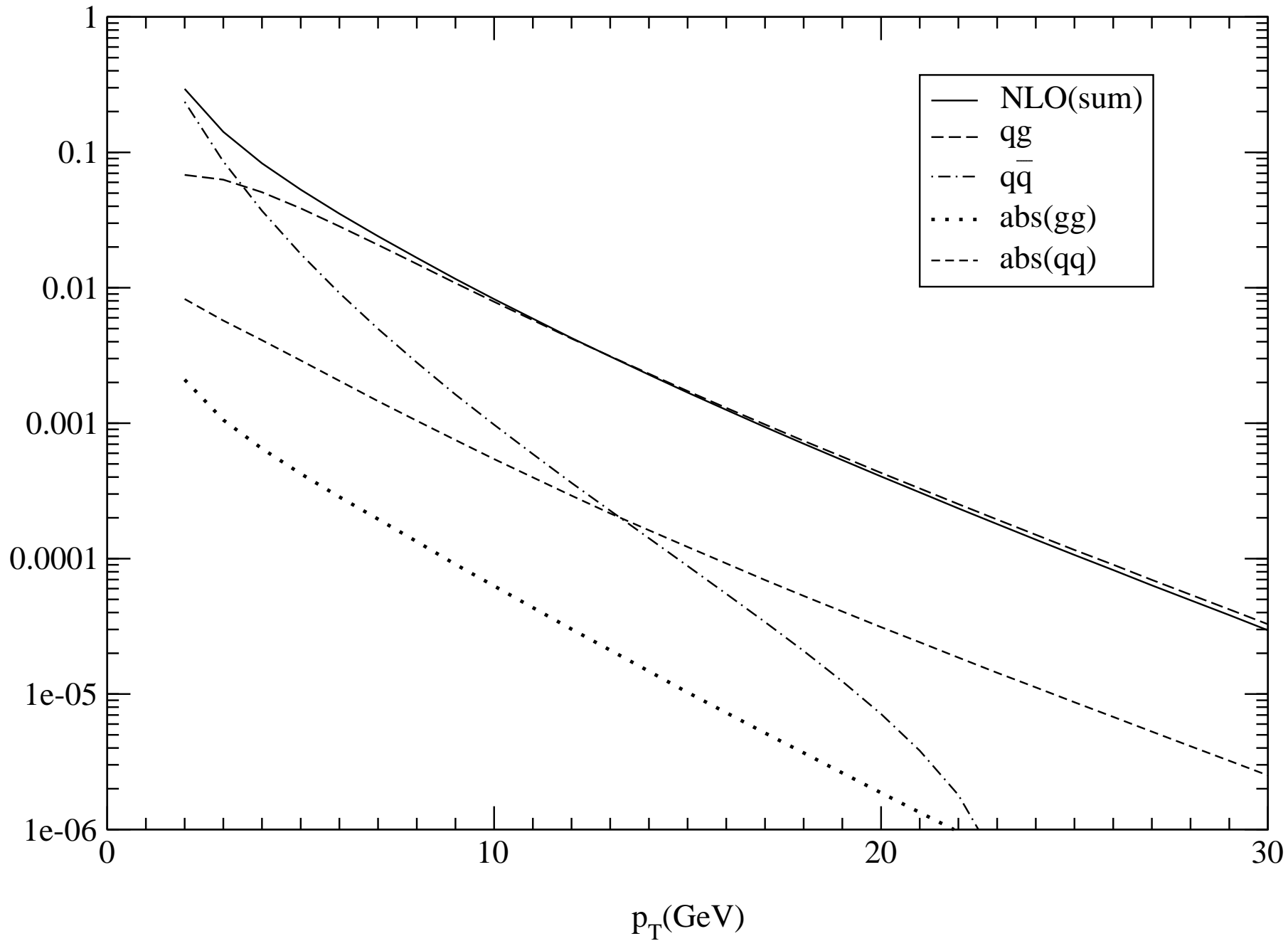
Fig. 10b. Same as in Fig. 10a but now for $A_{LL}(p_T, y)$ (Eq. (4.7)) in NLO.

Fig. 10c. The ratio of $A_{LL}(p_T, y)$ in NLO in Fig. 10b divided by $A_{LL}(p_T, y)$ in LO in Fig. 10a.

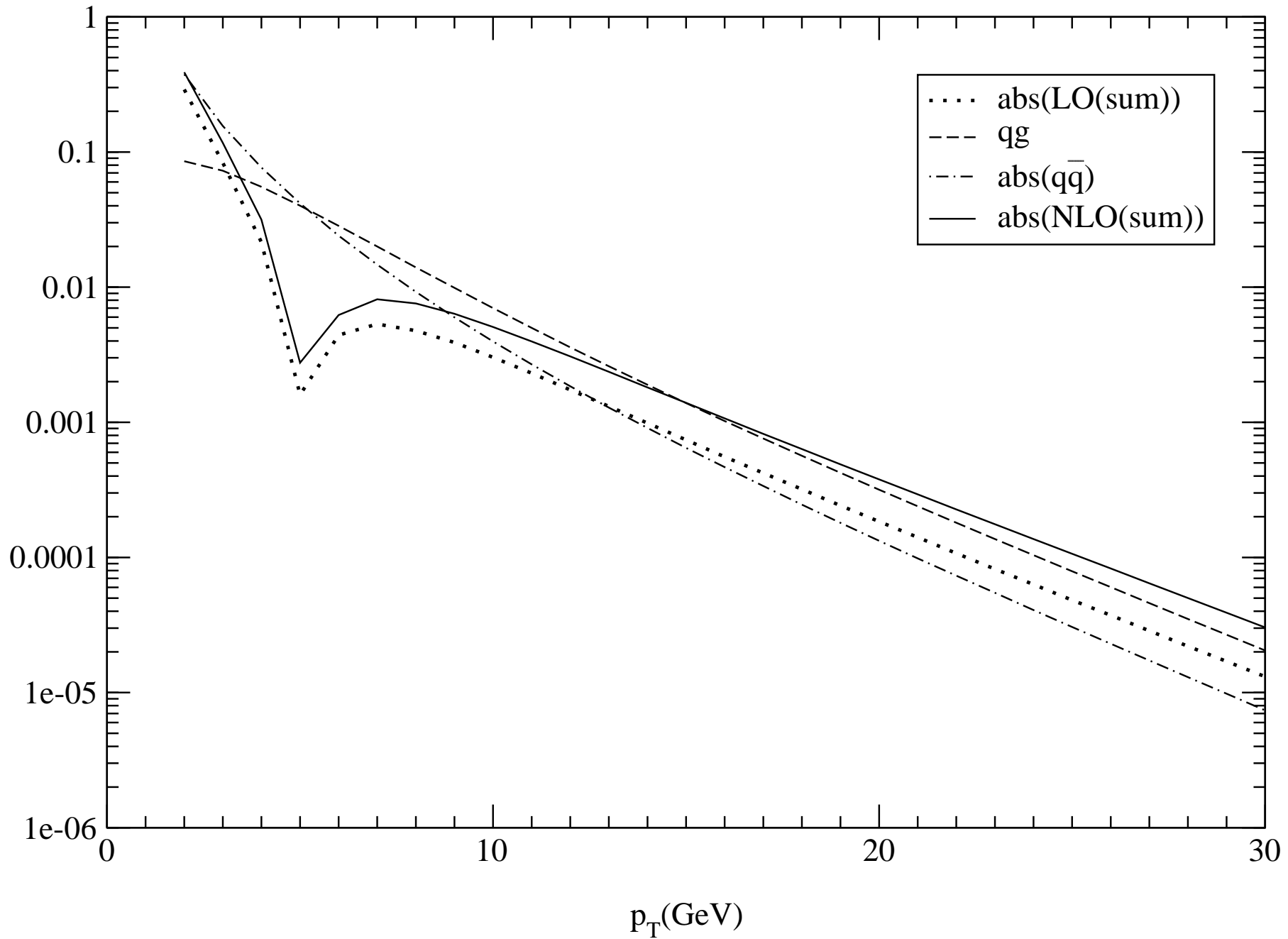
$$d^2 \Delta\sigma/dQdp_T(\text{pb}/\text{GeV}^2)$$



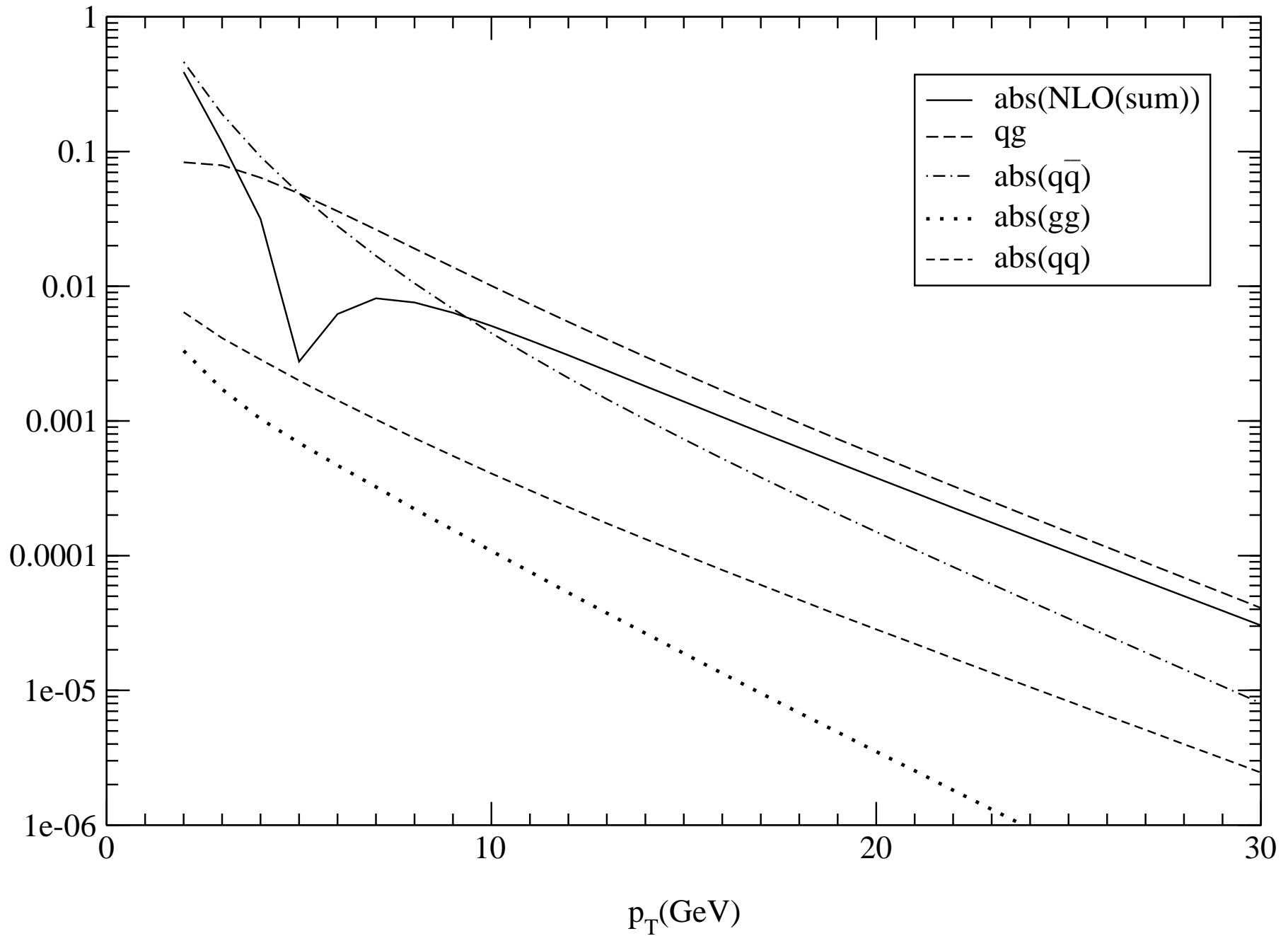
$$d^2 \Delta\sigma/dQdp_T(\text{pb}/\text{GeV}^2)$$



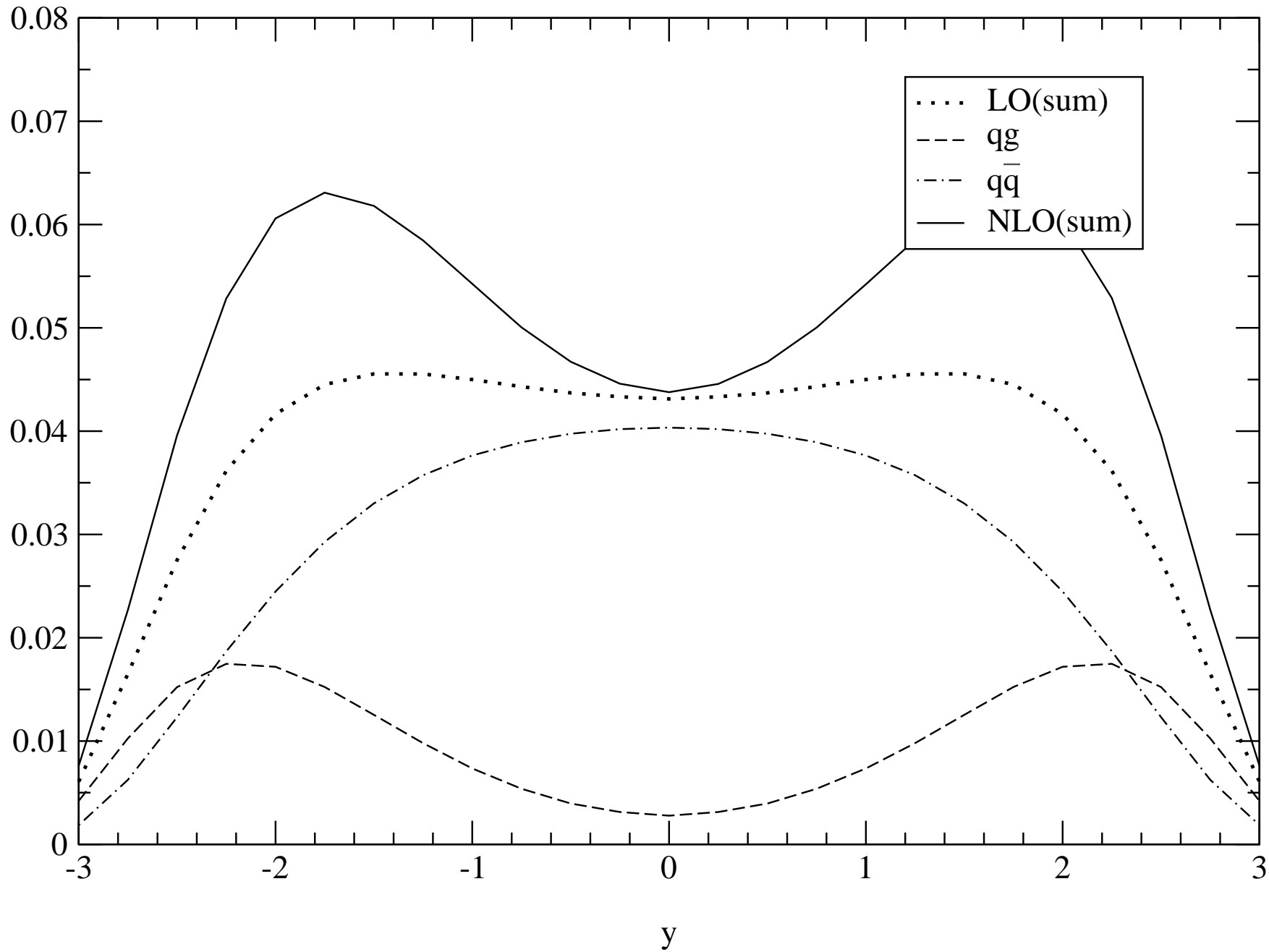
$$d^2 \Delta\sigma/dQdp_T(\text{pb}/\text{GeV}^2)$$



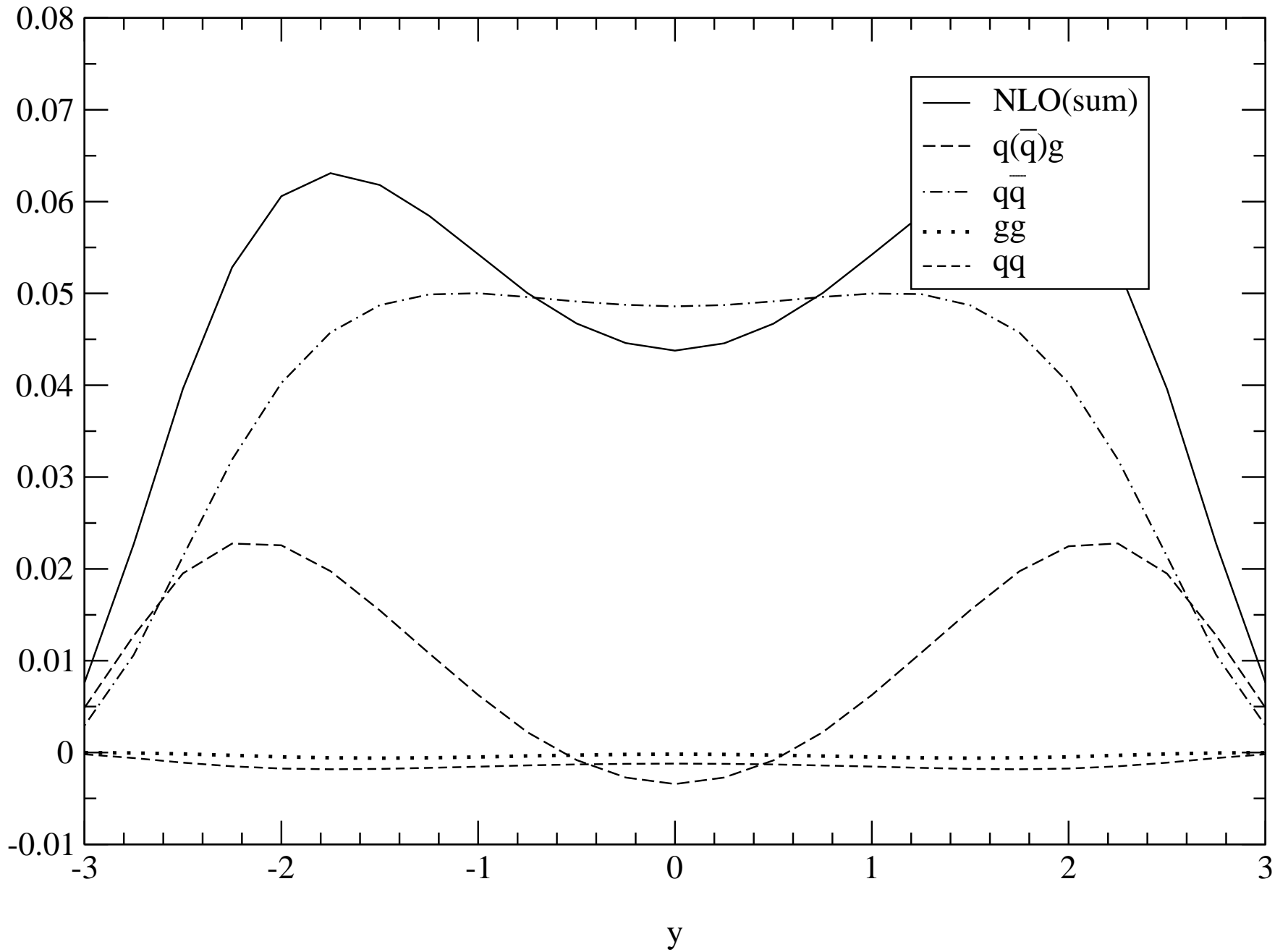
$$d^2 \Delta\sigma/dQdp_T(\text{pb}/\text{GeV}^2)$$



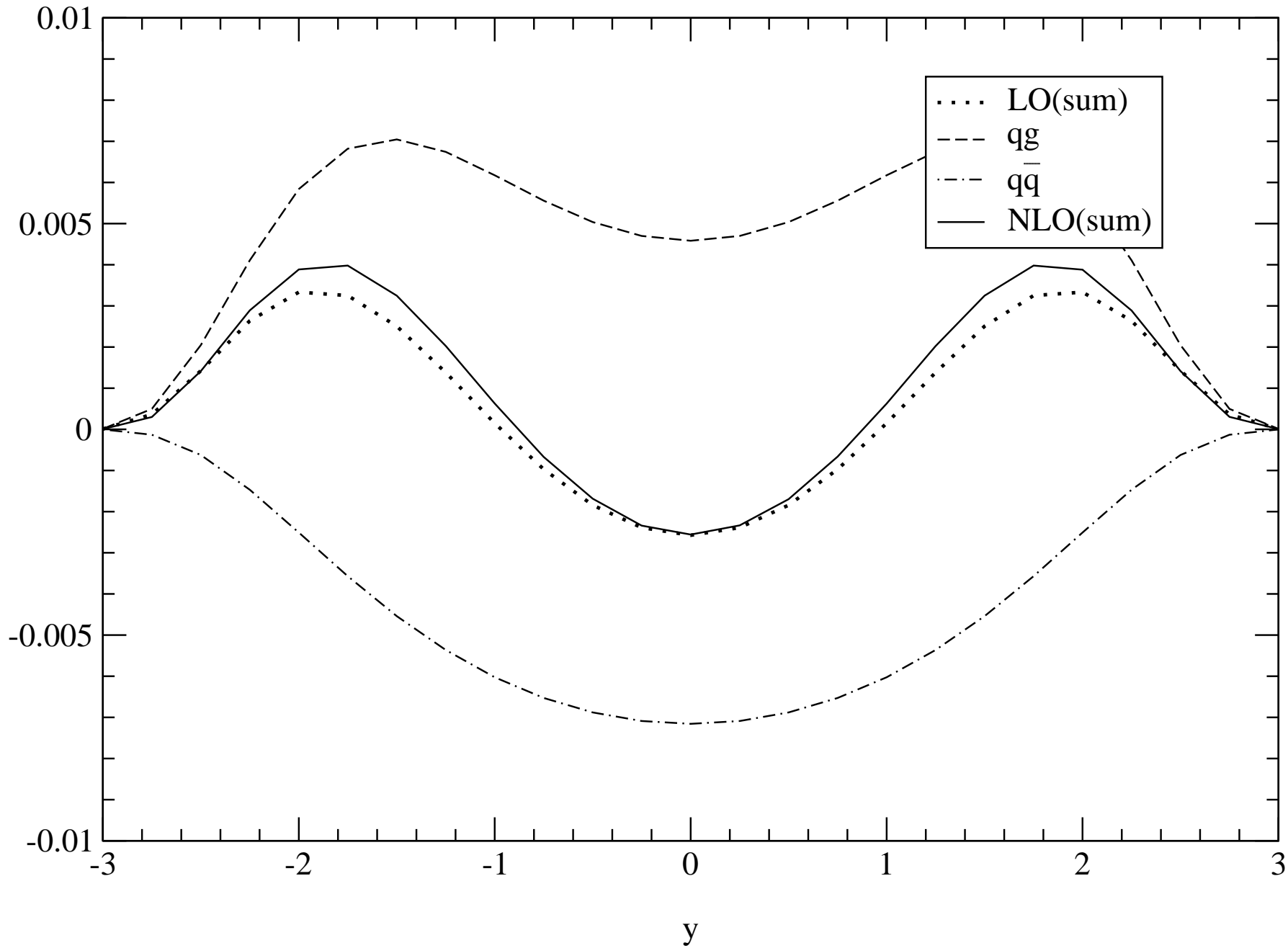
$$d^3 \Delta\sigma/dQdy(\text{pb/GeV})$$



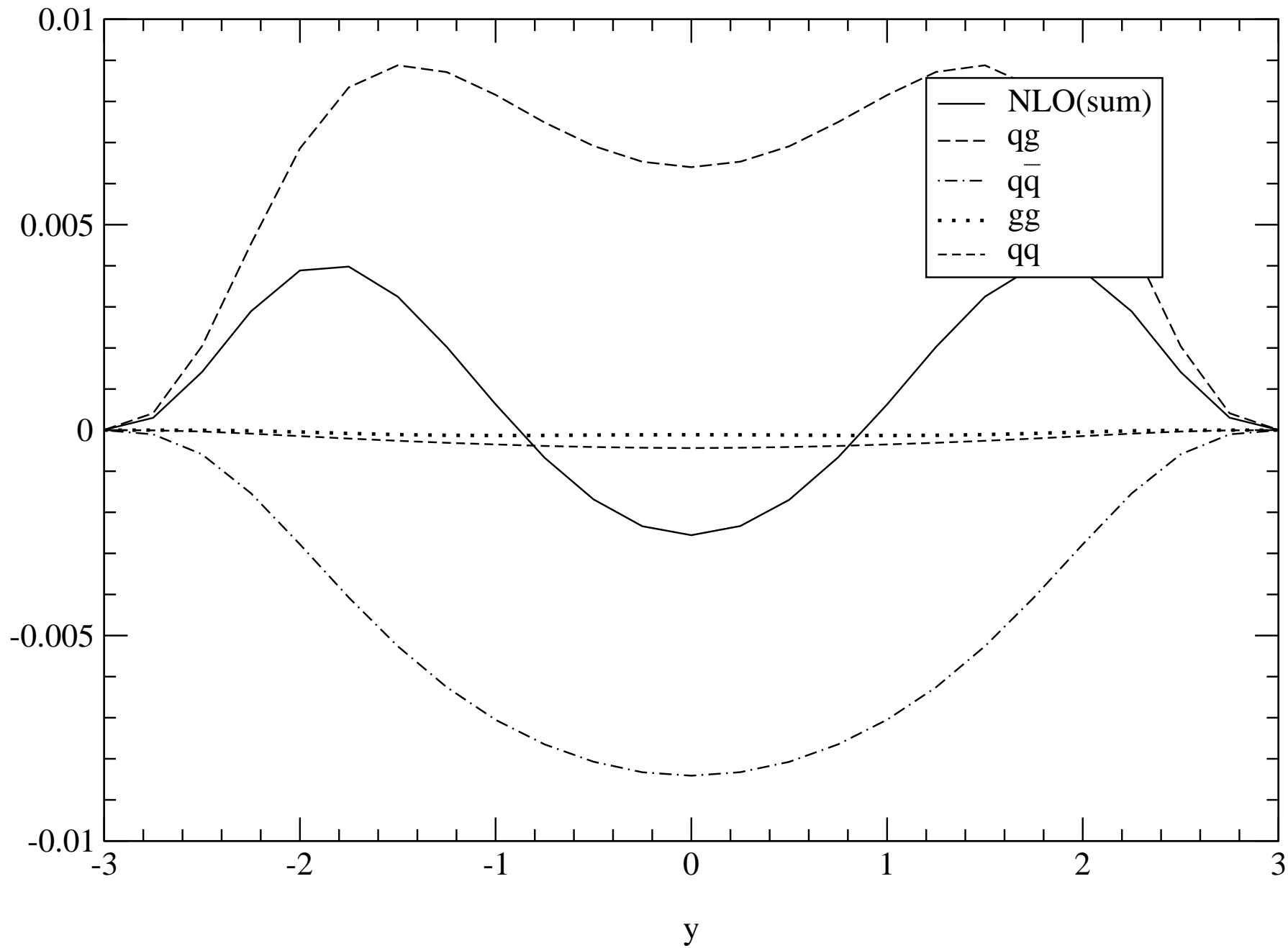
$$d^3 \Delta\sigma/dQdy(\text{pb/GeV})$$



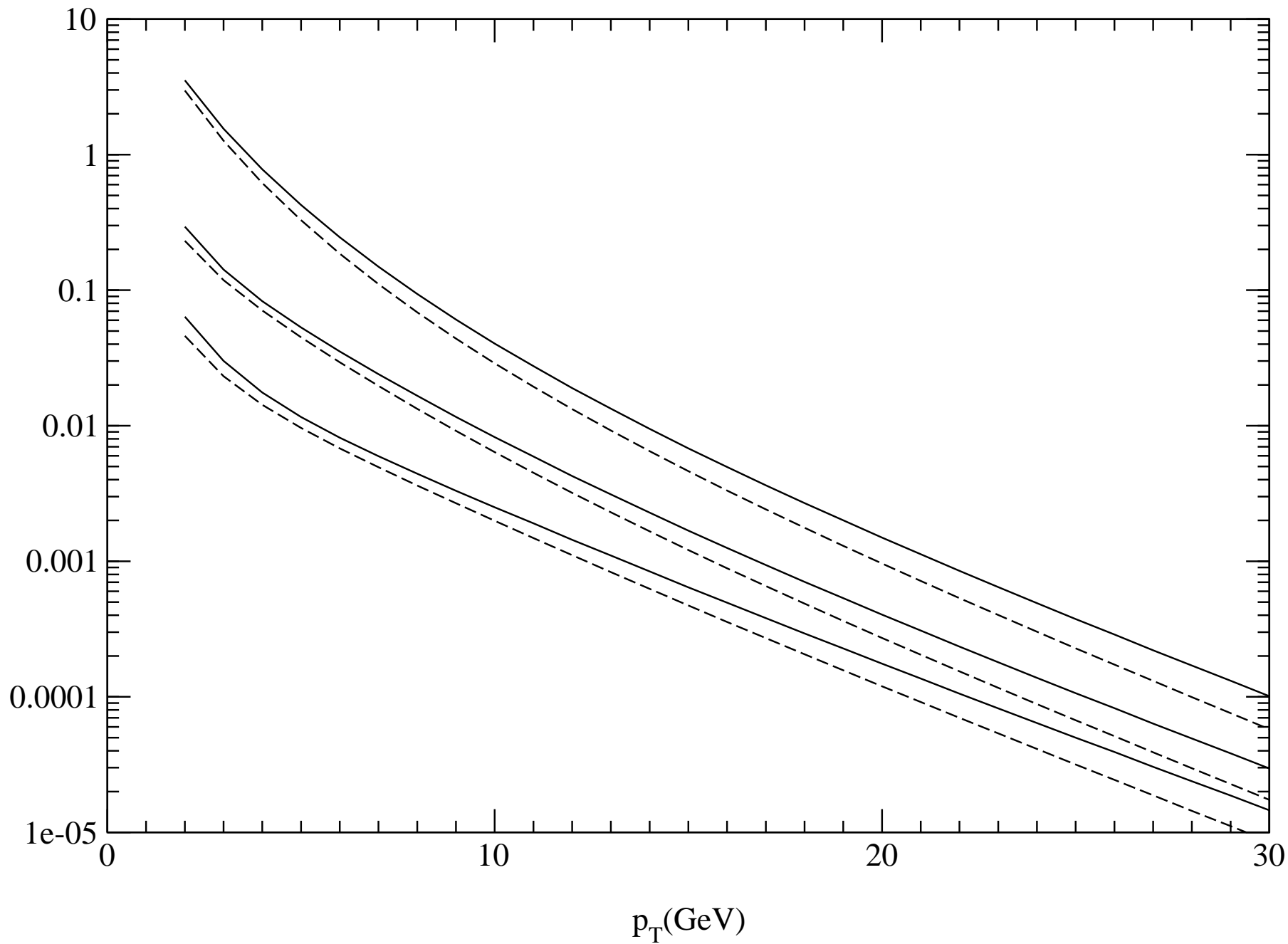
$$d^3 \Delta\sigma/dQdy(\text{pb/GeV})$$



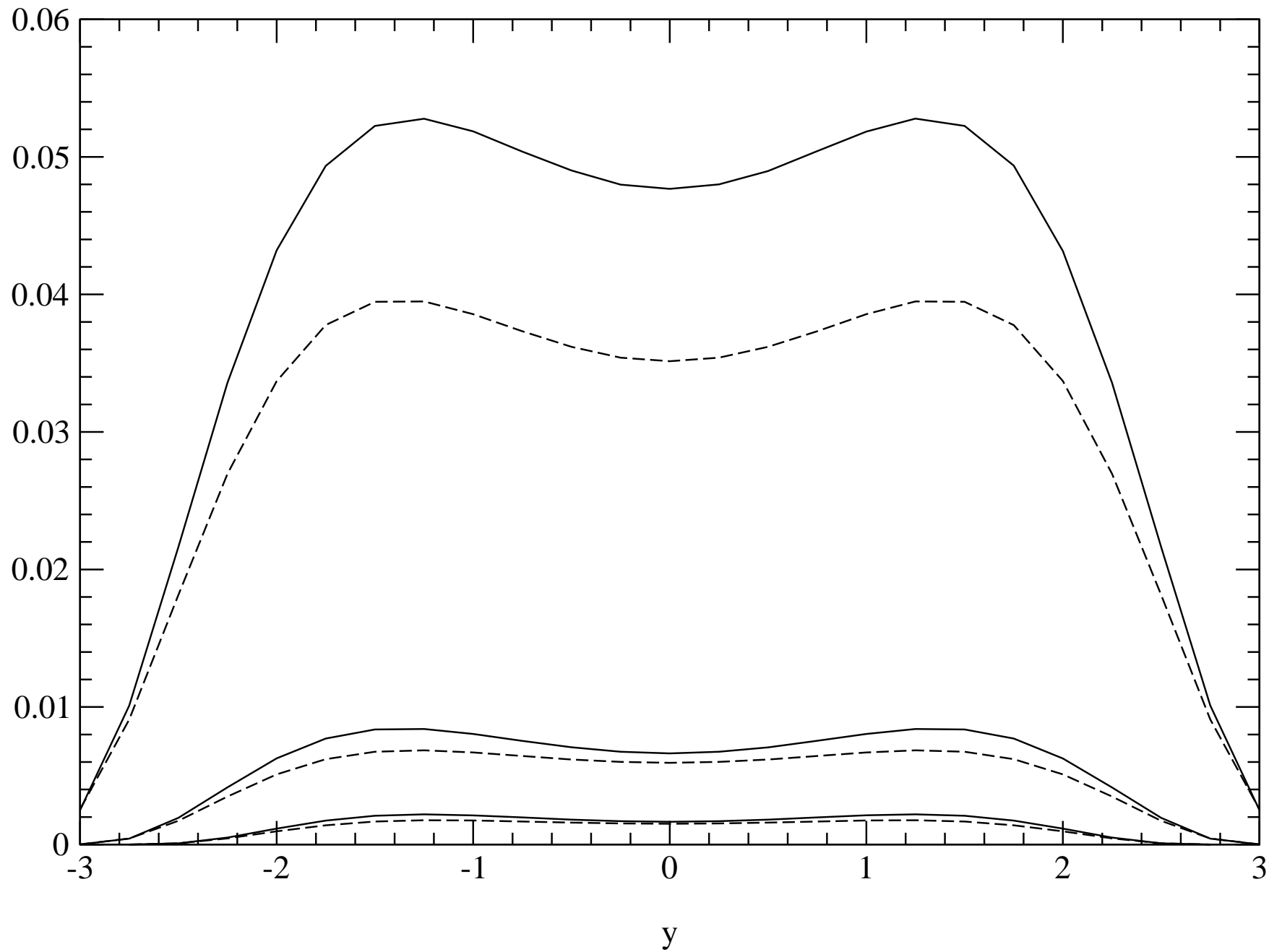
$$d^3 \Delta\sigma/dQdy(\text{pb/GeV})$$



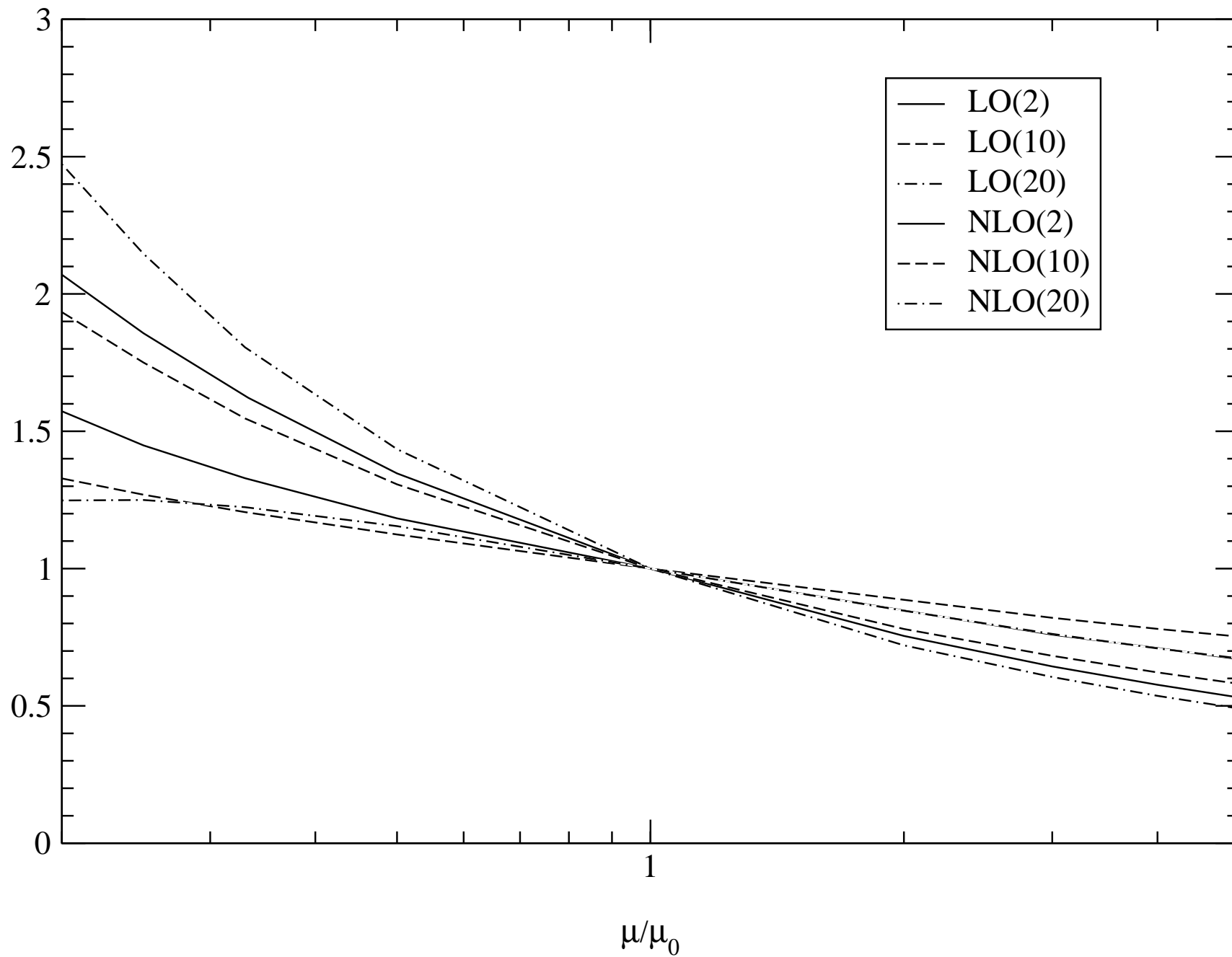
$$d^2 \Delta\sigma/dQdp_T(\text{pb}/\text{GeV}^2)$$



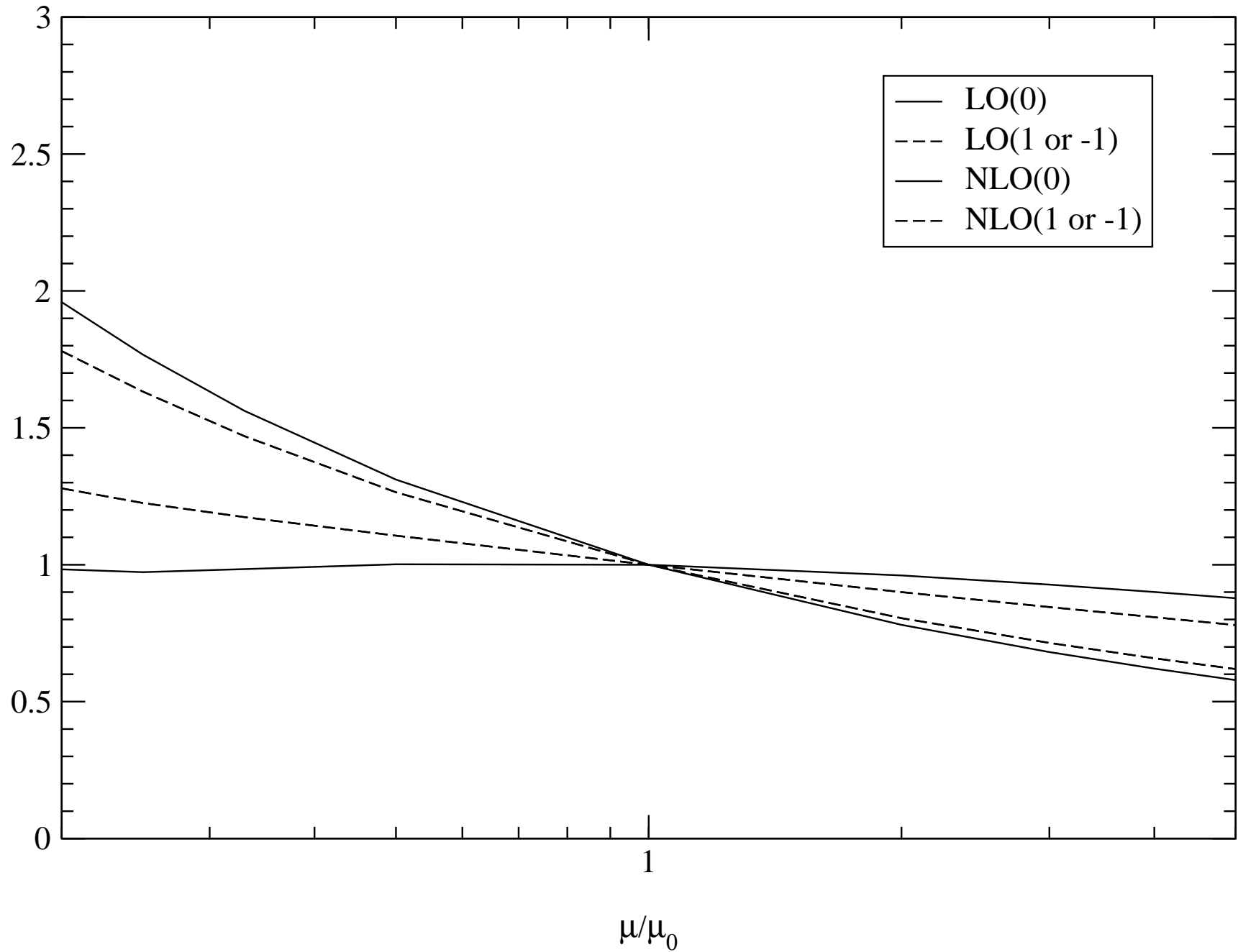
$$d^3\sigma/dQdy(\text{pb/GeV})$$



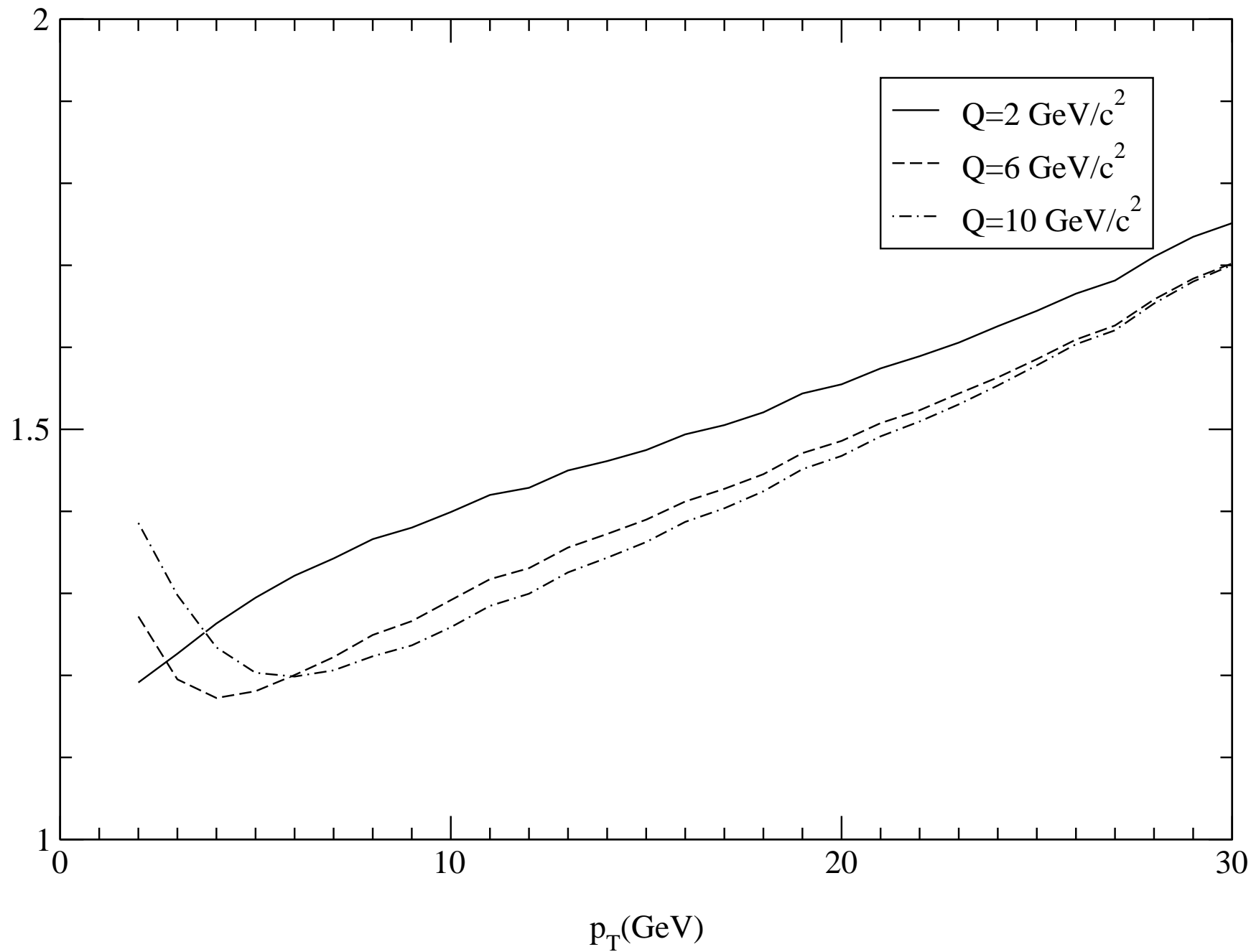
$$N(p_T, \mu/\mu_0)$$



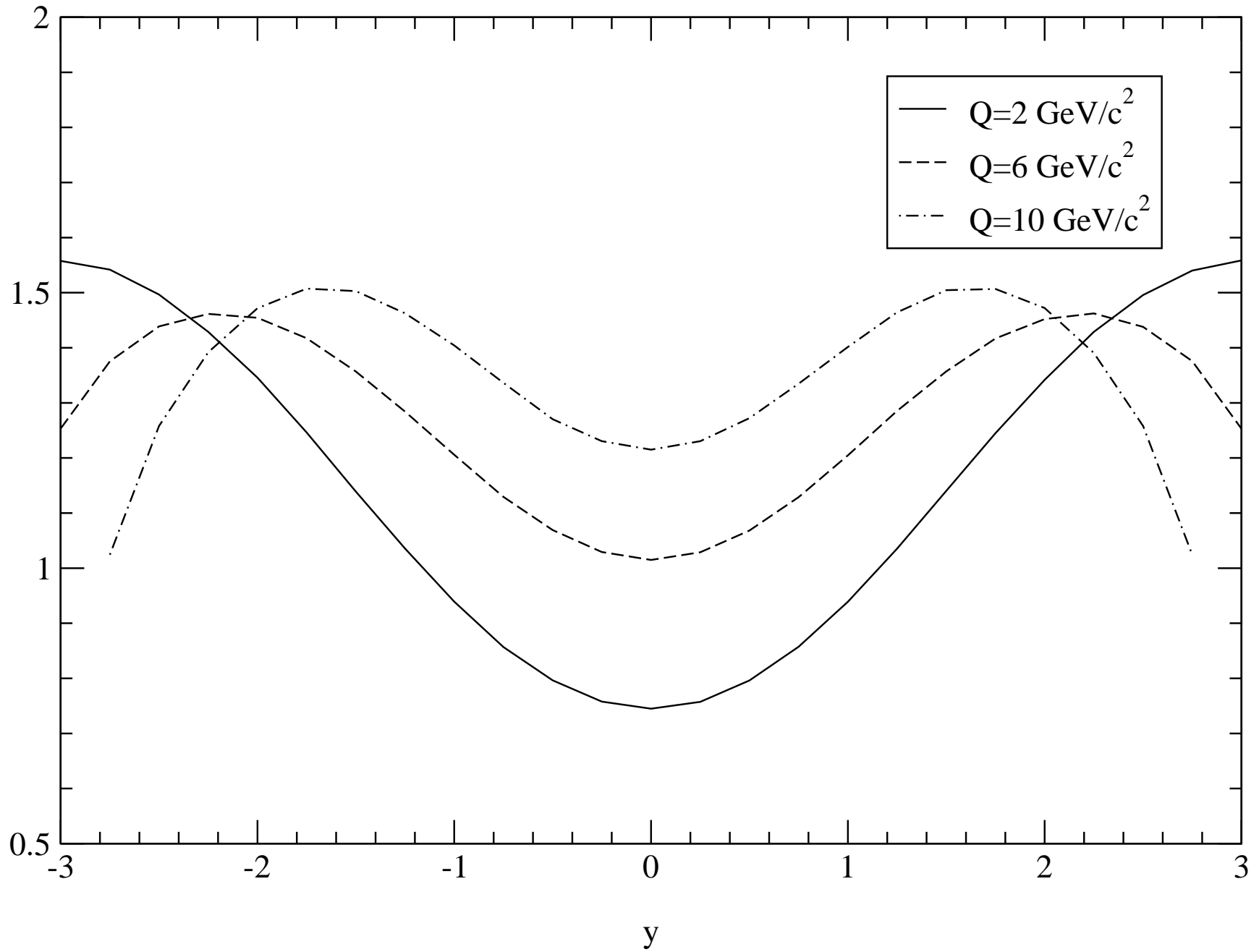
$$N(p_T, y, \mu/\mu_0)$$



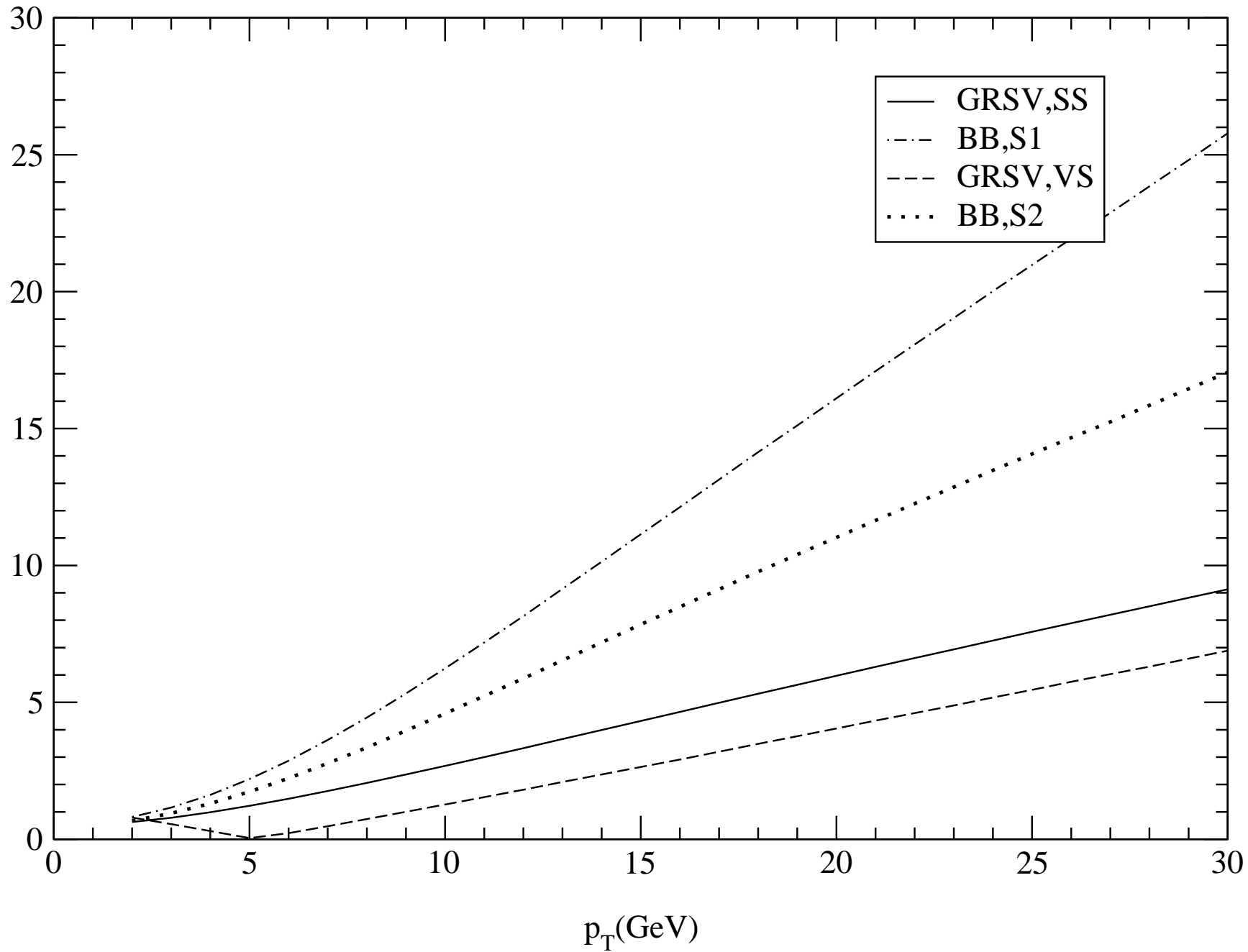
K= NLO/LO



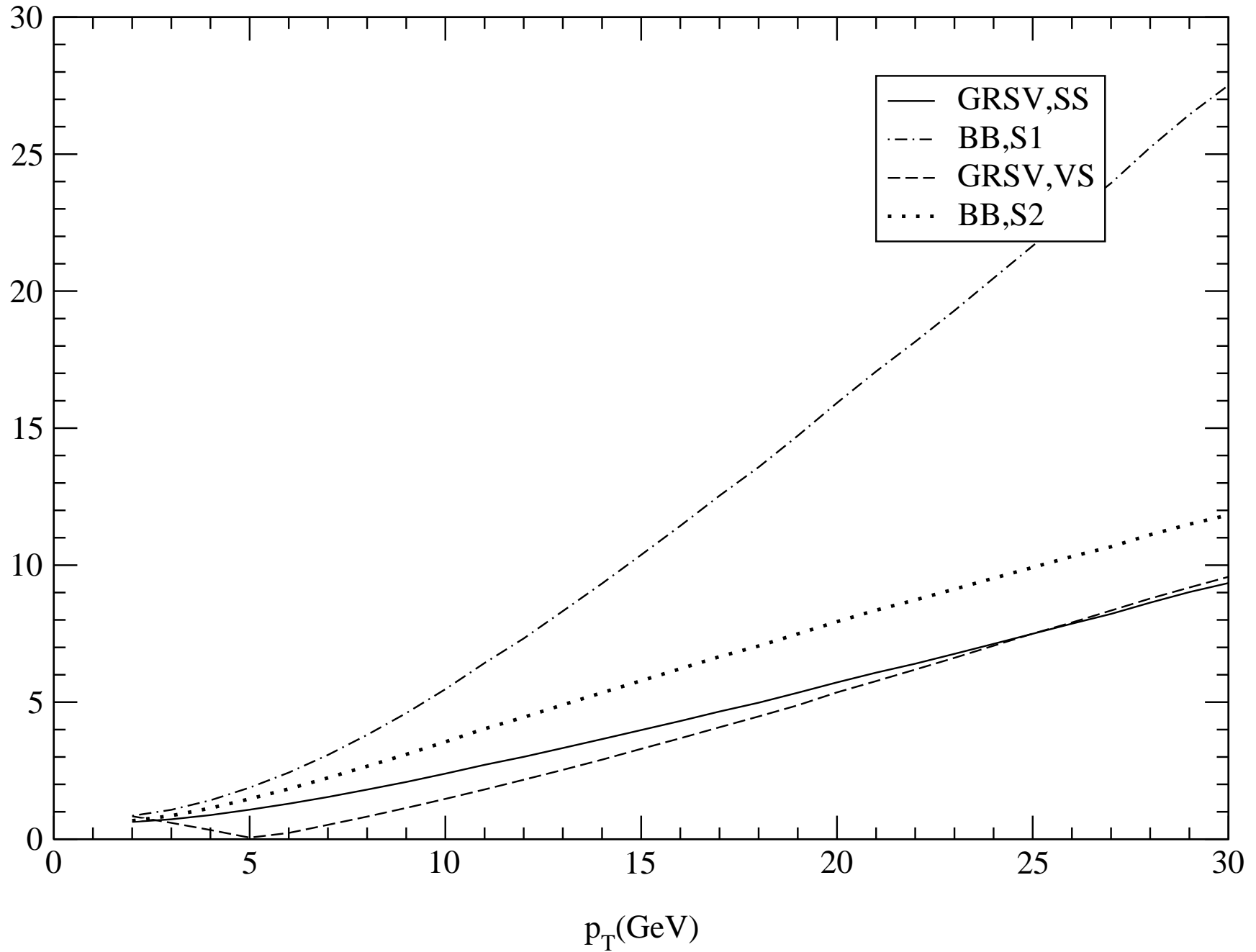
K=NLO/LO



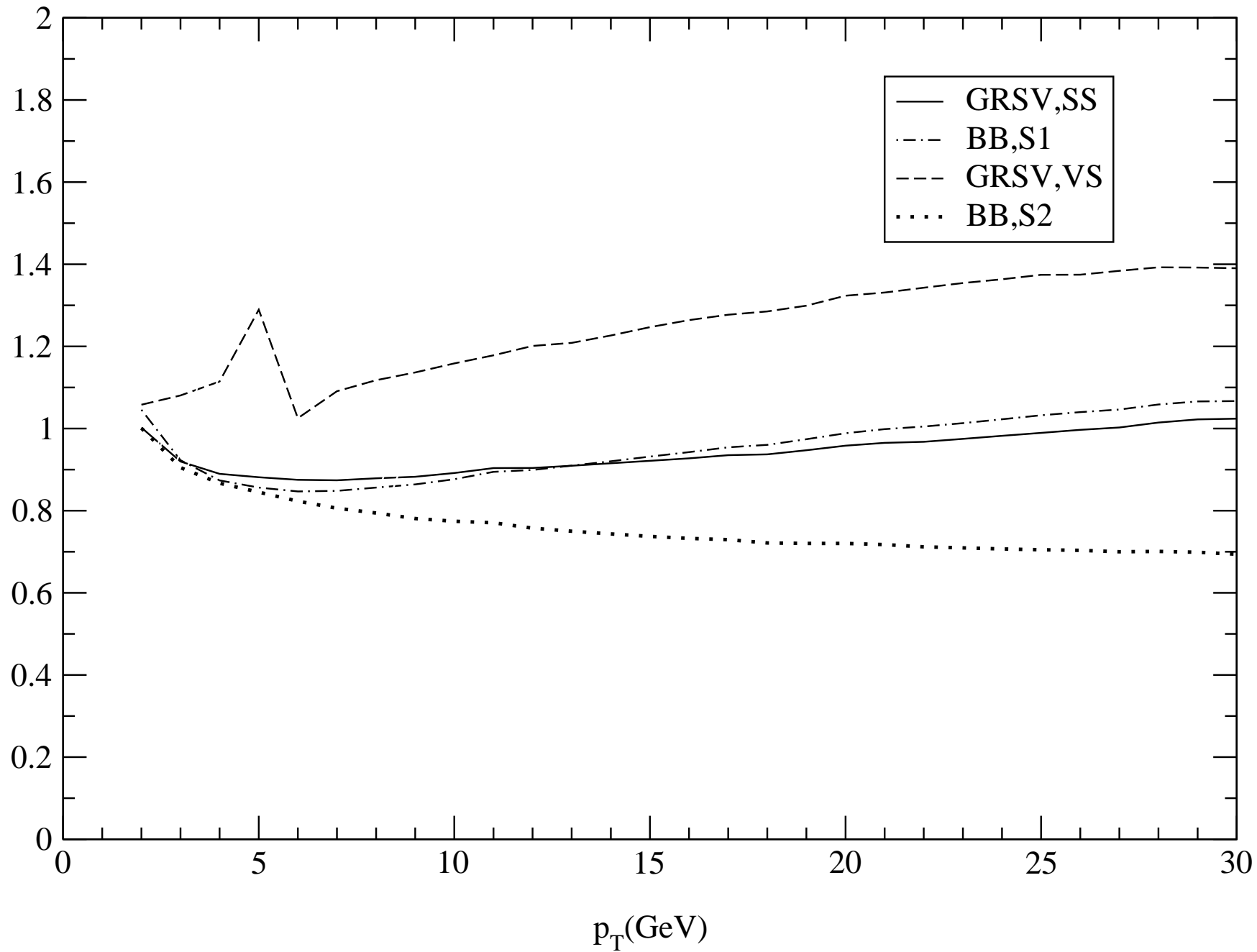
100*A_LL(LO)



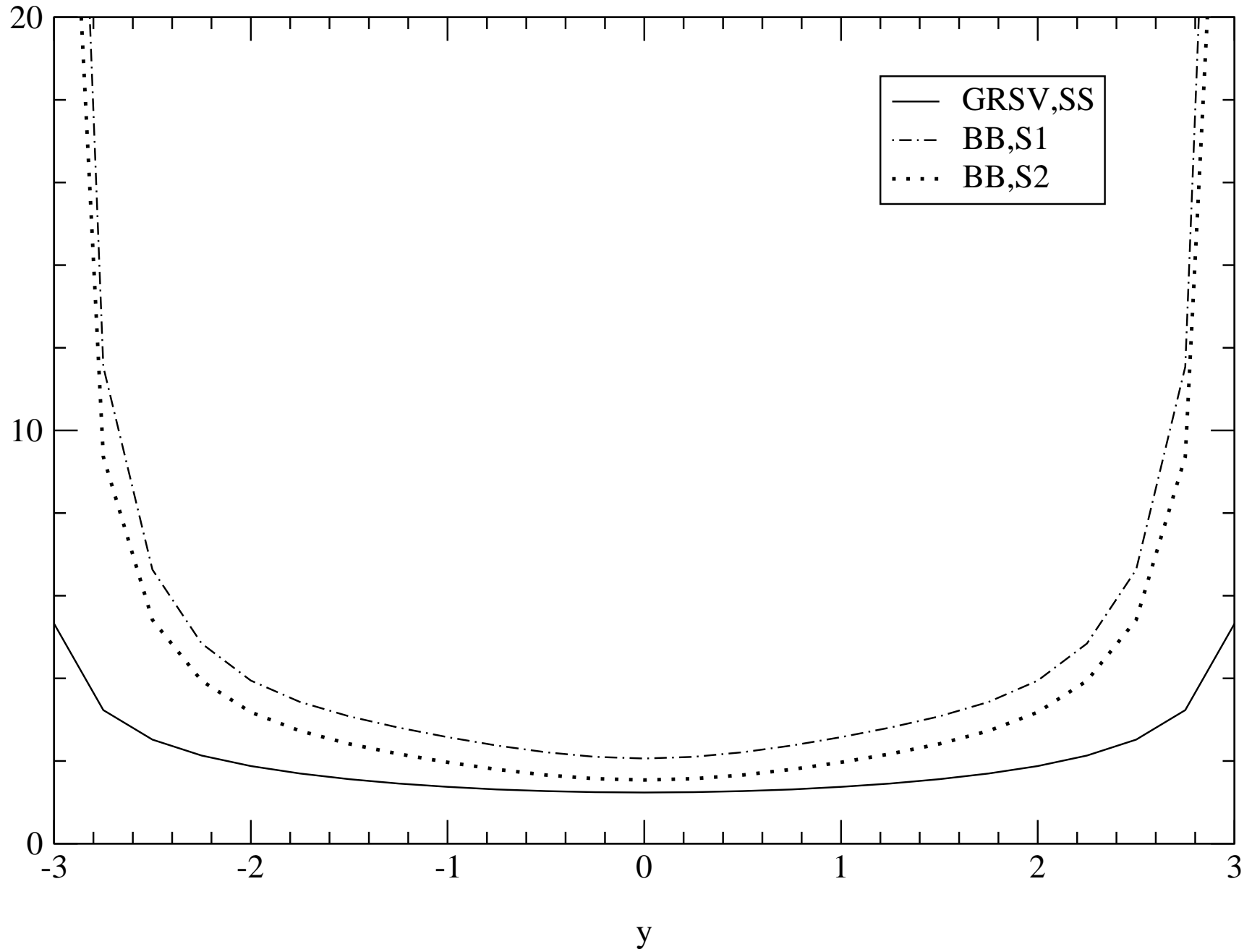
100*A_LL(NLO)



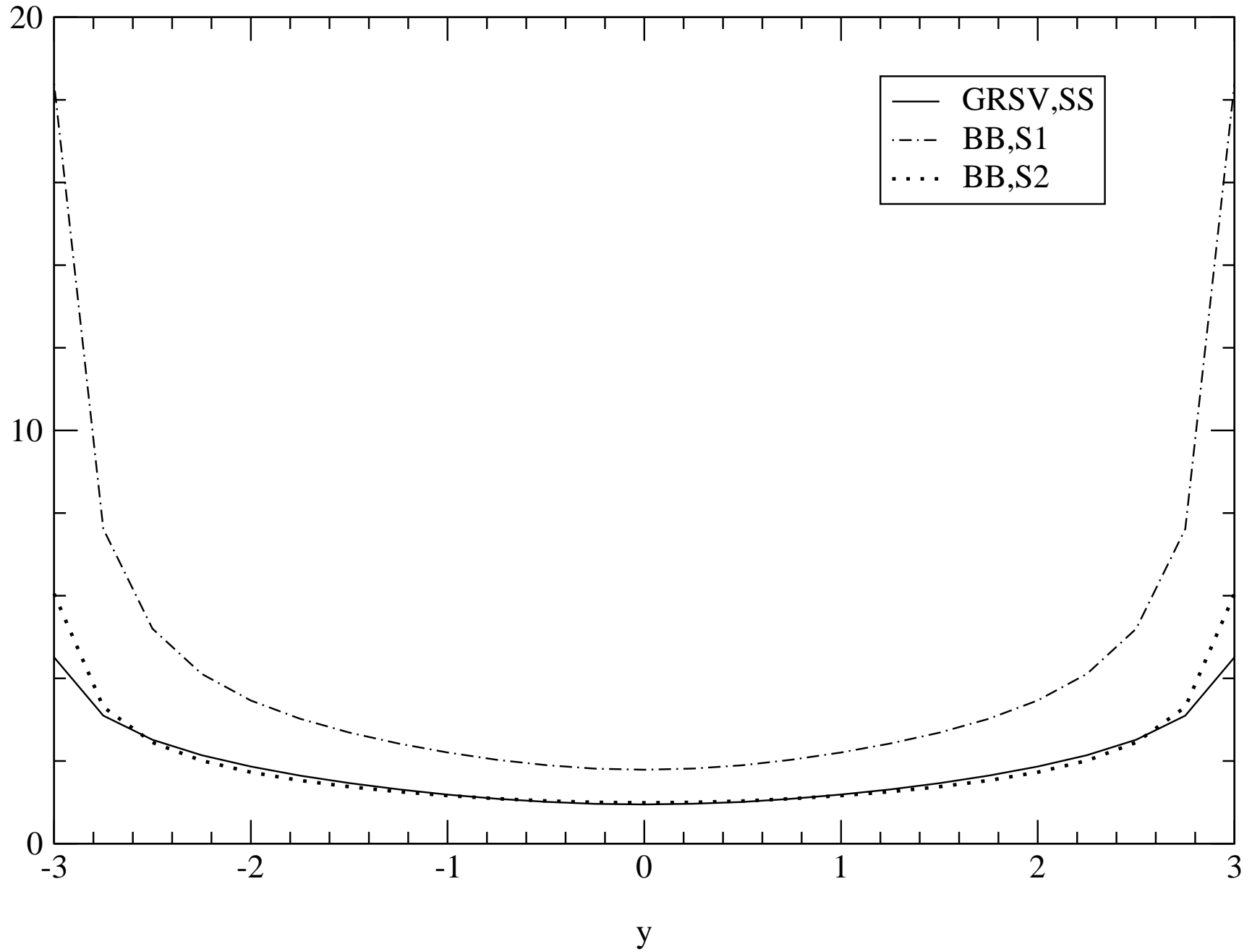
A_LL(NLO)/A_LL(LO)



$100 * A_{LL}(LO)$



100*A_LL(NLO)



A_LL(NLO)/A_LL(LO)

